

Low-Mass Higgs Bosons in the NMSSM and Their LHC Implications

Neil Christensen,^a Tao Han,^a Zhen Liu^a and Shufang Su^b

^a*Pittsburgh Particle physics, Astrophysics, and Cosmology Center, Department of Physics & Astronomy, University of Pittsburgh, 3941 O'Hara St., Pittsburgh, PA 15260, USA*

^b*Department of Physics, University of Arizona, P.O.Box 210081, Tucson, AZ 85721, USA*

E-mail: neilc@pitt.edu, than@pitt.edu, zhl61@pitt.edu,
shufang@physics.arizona.edu

ABSTRACT: We study the Higgs sector of the Next to Minimal Supersymmetric Standard Model (NMSSM) in light of the discovery of the SM-like Higgs boson at the LHC. We perform a broad scan over the NMSSM parameter space and identify the regions that are consistent with current Higgs search results at colliders. In contrast to the commonly studied “decoupling” scenario in the literature where the Minimal Supersymmetric Standard Model CP-odd Higgs boson mass is large $m_A \gg m_Z$, we pay particular attention to the light Higgs states in the case when $m_A \lesssim 2m_Z$. The Higgs bosons in the NMSSM, namely three CP-even states, two CP-odd states, and two charged Higgs states, could all be rather light, near or below the electroweak scale, although the singlet-like states can be heavier. The SM-like Higgs boson could be either the lightest CP-even scalar or the second lightest CP-even scalar, but is unlikely to be the heaviest scalar. These NMSSM parameter regions have unique properties and offer rich phenomenology. The decay branching fractions for the SM-like Higgs boson may be modified appreciably. The correlations of $\gamma\gamma/VV$ and $VV/b\bar{b}$ can be substantially altered. The new Higgs bosons may be readily produced at the LHC and may decay to non-standard distinctive final states, most notably a pair of Higgs bosons when kinematically accessible. We evaluate the production and decay of the Higgs bosons and comment on further searches at the LHC to probe the Higgs sector of the NMSSM.

Contents

1	Introduction	2
2	NMSSM Higgs Sector and the Low-m_A Region	4
2.1	Masses	5
2.1.1	CP-odd Higgs Bosons	5
2.1.2	Charged Higgs Bosons	5
2.1.3	CP-even Higgs Bosons	6
2.2	Low- m_A Region	7
2.3	Couplings	9
3	Parameter Scan and Constrained Regions	10
4	H_1 as the SM-like Higgs Boson	13
4.1	Parameter Regions	13
4.2	Production Cross Sections and Decay Branching Fractions of the SM-like H_1	18
4.3	Wave Function Overlap	20
5	H_2 as the SM-like Higgs Boson	22
5.1	Parameter Regions	22
5.2	Production Cross Sections and Decay Branching Fractions for the SM-like H_2	23
5.3	Wave Function Overlap	26
6	LHC Phenomenology for the Non-SM-like Higgs Bosons	26
6.1	H_1 as the SM-like Higgs Boson	26
6.2	H_2 as the SM-like Higgs Boson	30
7	Summary and Conclusions	33

1 Introduction

The Minimal Supersymmetric Standard Model (MSSM) remains one of the most appealing models that leads to a more complete theory beyond the Standard Model (SM). Its simplest extension, the Next to Minimal Supersymmetric Standard Model (NMSSM) [1, 2] introduces additional appealing features. Among the most notable is that it provides an attractive solution to the SUSY μ problem [3]. Furthermore, it is widely believed that the discovery of a Standard Model-like Higgs boson [4, 5] strongly supports the idea of weak-scale supersymmetry (SUSY) based on the “naturalness” argument. However, in the context of the MSSM, a Higgs mass of $m_h \sim 126$ GeV still requires a significant degree of fine tuning [6–9]. In contrast, the NMSSM largely alleviates the tuning required to achieve this rather high mass value [10, 11].

The Higgs sector of the MSSM consists of two $SU(2)_L$ doublets. After electroweak symmetry breaking (EWSB), there are five physical states left in the spectrum, two CP-even states h^0 and H^0 with $m_{h^0} < m_{H^0}$, one CP-odd state A^0 , and two charged scalar states H^\pm . At tree-level, it is customary to use the mass m_A and the ratio of the vacuum expectation values $\tan\beta = v_u/v_d$ as the free parameters to determine the other masses. These masses receive large radiative corrections from the top-stop sector due to the large top Yukawa coupling. If we categorize these Higgs bosons according to their couplings to the electroweak gauge bosons, there are two distinct regions in the MSSM [12]:

- (i) The “decoupling region”: For a relatively heavy A^0 ($m_A \gtrsim 300$ GeV), the lighter CP-even state h^0 is the SM-like Higgs and the others H^0 , A^0 , and H^\pm are heavy and nearly degenerate.
- (ii) The “non-decoupling region”: For $m_A \sim m_Z$, the heavier CP-even Higgs H^0 is the SM-like Higgs, while h^0 and A^0 are light and nearly degenerate. The mass of the charged Higgs H^\pm is typically around 140 GeV.

The decoupling scenario comfortably accommodates the current searches due to the effective absence of the non-SM-like Higgs states. In fact, it would be very difficult to observe any of the heavy MSSM Higgs bosons at the LHC if $m_A \gtrsim 400$ GeV for a modest value of $\tan\beta \lesssim 10$ [13–16]. The non-decoupling scenario, on the other hand, would lead to a rich LHC phenomenology due to the existence of multiple light Higgs bosons. Although this latter scenario would be more tightly constrained by current experiments, it would correspondingly have greater predictive power for its phenomenology.

In the NMSSM, one complex $SU(2)_L \times U(1)_Y$ singlet scalar field is added to the Higgs sector. As a result, after the scalar fields acquire vacuum expectation values, one new CP-even and one new CP-odd state are added to the MSSM spectrum, resulting in three CP-even mass eigenstates (denoted by H_1 , H_2 , H_3), two CP-odd mass eigenstates (A_1 , A_2), plus a pair of charged states (H^\pm).

The masses of the CP-even scalars can be better understood by considering what happens when the singlet is added to the MSSM spectrum. The masses of the MSSM Higgs bosons can be in one of two scenarios: the SM-like Higgs of the MSSM can either be

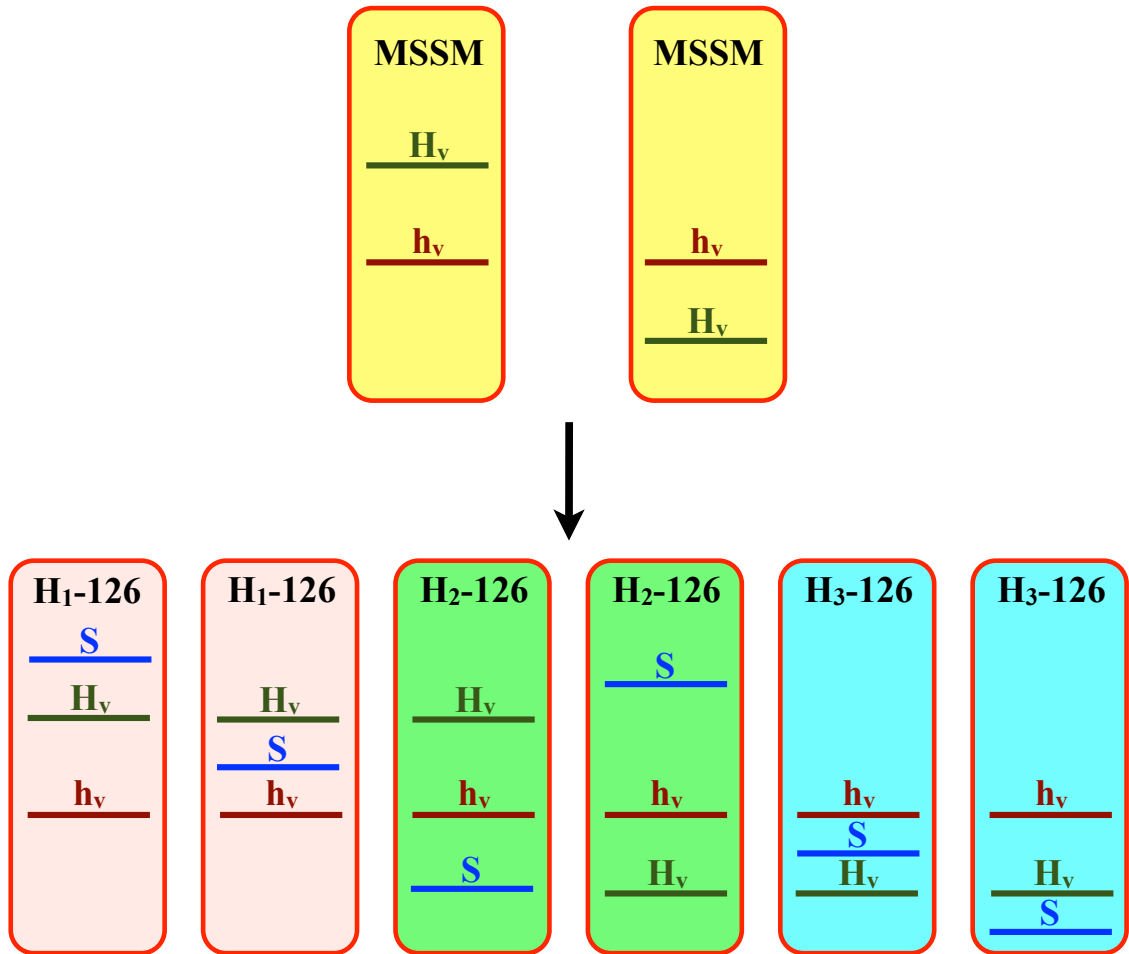


Figure 1. Illustration of the effect of adding the singlet to the MSSM CP-even Higgs boson spectrum before mixing.

the lighter eigenstate or the heavier eigenstate, as illustrated in the top row of Fig. 1. After adding the singlet scalar, the two panels of the MSSM give rise to six possible scenarios in the NMSSM, as illustrated in the lower row of Fig. 1. In reality, the mass eigenstates are admixtures of the gauge interaction eigenstates, and thus cannot be labelled as simply as in Fig. 1. Nevertheless, these graphs give us an intuitive picture of the result of adding the singlet field of the NMSSM.

Recently, many analyses of the NMSSM have been performed in light of the recent Higgs searches at the LHC, focusing on the large m_A region. References [17–19] showed the compatibility of the NMSSM with an enhanced $\gamma\gamma$ rate, while Reference [20] studied the stringent flavor and muon $g - 2$ constraints on the model. Moreover, the NMSSM may include many interesting features, that include grand unification of gauge couplings [21], naturalness for the Higgs mass [10, 11, 22–24], neutralino Dark Matter [25–27], and possible accommodation of multiple nearly degenerate Higgs bosons [28–30].

In this paper, by contrast, we consider the NMSSM in the *low- m_A* region, the prototype

of which is the non-decoupling scenario of the MSSM. We perform a broad scan over the NMSSM parameter space and identify the low- m_A regions that are consistent with current Higgs search results at the colliders, including the discovery of a SM-like Higgs boson. We find that the Higgs bosons of the NMSSM, three CP-even states, two CP-odd states, and two charged Higgs states, could all be rather light, near or below the electroweak scale in our low- m_A scenario, although the singlet-like states can also be heavier. The SM-like Higgs boson could be either the lightest scalar or the second lightest scalar, as illustrated in panels 1 – 4 of the bottom row of Fig. 1. However, it is extremely difficult to uncover any regions corresponding with the scenarios of the last two panels of Fig. 1 where the SM-like Higgs boson is the heaviest CP-even state after imposing all the existing collider search constraints.

These low- m_A parameter regions of the NMSSM have unique properties and offer rich phenomenology, providing complementary scenarios to the existing literature for the large- m_A case, as mentioned above. The production cross section and decay branching fractions for the SM-like Higgs boson may be modified appreciably and new Higgs bosons may be readily produced at the LHC. We evaluate the production and decay of the Higgs bosons in this model and propose further searches at the LHC to probe the Higgs sector of the NMSSM.

The rest of this paper is organized as follows. In Sec. 2, we present a short, self-contained introduction to the Higgs sector of the NMSSM. In Sec. 3, we discuss our parameter scanning scheme and the current constraints applied. We then discuss the resulting constraints and correlations for the NMSSM parameter space in Sec. 4 for the case that the SM-like Higgs is the lightest CP-even scalar (panels 1-2, bottom row of Fig. 1) and in Sec. 5 when the SM-like Higgs is the second lightest CP-even scalar (panels 3-4, bottom row of Fig. 1). In Sec. 6, we consider the basic LHC phenomenology for our results. Finally, we summarize and conclude in Sec. 7.

2 NMSSM Higgs Sector and the Low- m_A Region

In the NMSSM [1, 2, 31, 32], a new gauge singlet chiral superfield $\hat{\mathcal{S}}$ is added to the MSSM Higgs sector resulting in a superpotential of the form

$$W_{\text{NMSSM}} = Y_u \hat{u}^c \hat{H}_u \hat{Q} + Y_d \hat{d}^c \hat{H}_d \hat{Q} + Y_e \hat{e}^c \hat{H}_d \hat{L} + \lambda \hat{\mathcal{S}} \hat{H}_u \hat{H}_d + \frac{1}{3} \kappa \hat{\mathcal{S}}^3 \quad (2.1)$$

with an explicit \mathbb{Z}_3 symmetry. Additionally, the soft-SUSY breaking Higgs sector of the NMSSM is:

$$V_{H,\text{Soft}} = m_{H_u}^2 H_u^\dagger H_u + m_{H_d}^2 H_d^\dagger H_d + M_S^2 |\mathcal{S}|^2 + \left(\lambda A_\lambda (H_t^T \epsilon H_d) \mathcal{S} + \frac{1}{3} \kappa A_\kappa \mathcal{S}^3 + c.c. \right). \quad (2.2)$$

After the singlet obtains a vacuum expectation value (VEV) $\langle \mathcal{S} \rangle = v_s / \sqrt{2}$, an effective μ term is generated: $\mu = \lambda v_s / \sqrt{2}$, which solves the so-called μ -problem of the MSSM. An effective b -term $b_{\text{eff}} = \mu (A_\lambda + \frac{\kappa}{\lambda} \mu)$ is also generated at tree level.

In this work, we assume a CP-conserving Higgs potential with all the coefficients being real. We further take λ and κ to be positive, unless otherwise stated. For the VEVs, we

use the convention $\langle H_u^0 \rangle = v_u/\sqrt{2}$, $\langle H_d^0 \rangle = v_d/\sqrt{2}$, with $v_u^2 + v_d^2 = v^2 = (246 \text{ GeV})^2$ and $\tan \beta = v_u/v_d$. After electroweak symmetry breaking, we are then left with three CP-even Higgs states H_1, H_2, H_3 , two CP-odd Higgs states A_1, A_2 , and a pair of charged Higgs states H^\pm .

2.1 Masses

2.1.1 CP-odd Higgs Bosons

For the CP-odd Higgs bosons, we define the mixing states

$$A_v = \sqrt{2} \left(\text{Im}(H_d^0) \sin \beta + \text{Im}(H_u^0) \cos \beta \right), \quad A_s = \sqrt{2} \text{Im}(\mathcal{S}). \quad (2.3)$$

The relevant parameters of our interest are the diagonal elements of the mass matrix in the basis of (A_v, A_s) as

$$m_A^2 = \frac{2\mu}{\sin 2\beta} \left(A_\lambda + \frac{\kappa}{\lambda} \mu \right) = \frac{2b_{\text{eff}}}{\sin 2\beta}, \quad (2.4)$$

$$m_{A_s}^2 = \frac{\lambda^2 v^2}{8\mu^2} \left(m_A^2 \sin 2\beta + 6 \frac{\kappa}{\lambda} \mu^2 \right) \sin 2\beta - 3 \frac{\kappa}{\lambda} \mu A_\kappa. \quad (2.5)$$

The full mass matrix expression can be found in Ref. [31]. In the limit of zero mixing between A_v and A_s , m_A is the mass of the CP-odd Higgs A_v , as in the case of the MSSM. However, in the NMSSM, the mass eigenstates are typically a mixture of A_v and A_s , resulting in a more complicated mass spectrum and parameter dependence. Although m_A is not a mass eigenvalue in the NMSSM, it takes the same form in terms of b_{eff} as in the MSSM [see Eq. (2.4)]. We also note that $m_{A_s}^2$ has the contribution $-3 \frac{\kappa}{\lambda} \mu A_\kappa$. As a result, to obtain positive mass squared eigenvalues, the combination μA_κ can not be too large and positive, in particular, for the small m_A region that we consider in this paper. We denote the mass eigenstates as A_1 and A_2 , where $m_{A_1} \leq m_{A_2}$.

2.1.2 Charged Higgs Bosons

The charged Higgs bosons H^\pm in the NMSSM have the same definition as in the MSSM, but a new contribution to their mass

$$H^\pm = H_d^\pm \sin \beta + H_u^\pm \cos \beta, \quad m_{H^\pm}^2 = m_A^2 + m_W^2 - \frac{1}{2}(\lambda v)^2. \quad (2.6)$$

The extra λ -dependent term leads to a reduction of the charged Higgs mass compared to its MSSM value. Requiring $m_{H^\pm}^2 \geq 0$ gives an upper bound for λ as a function of m_A

$$\lambda \leq \frac{\sqrt{2}}{v} \sqrt{m_A^2 + m_W^2}. \quad (2.7)$$

The LEP search limit $m_{H^\pm} \gtrsim 80 \text{ GeV}$ [33, 34], as well as the bounds from the Tevatron and LHC charged Higgs boson searches, strengthen this upper limit even further, depending on the value of $\tan \beta$.

2.1.3 CP-even Higgs Bosons

The CP-even Higgs sector is much more complicated compared to that of the MSSM. It is advantageous to define the basis as:

$$\begin{pmatrix} h_v \\ H_v \end{pmatrix} = \begin{pmatrix} \cos \beta & \sin \beta \\ -\sin \beta & \cos \beta \end{pmatrix} \begin{pmatrix} \sqrt{2} (\text{Re}(H_d^0) - v_d) \\ \sqrt{2} (\text{Re}(H_u^0) - v_u) \end{pmatrix}, \quad S = \sqrt{2} (\text{Re}(S) - v_s). \quad (2.8)$$

The benefit of using this basis is that the couplings of h_v to the gauge sector and the fermion sector are exactly *the same* as that of the SM Higgs. On the other hand, H_v does *not* couple to pairs of gauge bosons at all, and its coupling to the up-type quarks (down-type quarks and charged leptons) is proportional to $\frac{1}{\tan \beta}$ ($\tan \beta$) with respect to the SM values. The singlet, S , does not couple to either the gauge bosons or the fermions. While the mass eigenstates $H_{1,2,3}$ (with $m_{H_1} \leq m_{H_2} \leq m_{H_3}$) are typically mixtures of h_v , H_v and S , by knowing the fraction of h_v , H_v , and S in the mass eigenstates, we have a better understanding of their interactions with the gauge bosons and fermions.

The diagonal entries of the mass matrix for the CP-even Higgs bosons in the basis of (h_v, H_v, S) are given by [31]

$$m_{h_v}^2 = m_Z^2 + \left[\frac{1}{2}(\lambda v)^2 - m_Z^2 \right] \sin^2 2\beta, \quad (2.9)$$

$$m_{H_v}^2 = m_A^2 - \left[\frac{1}{2}(\lambda v)^2 - m_Z^2 \right] \sin^2 2\beta, \quad (2.10)$$

$$m_S^2 = \frac{\lambda^2 v^2}{8\mu^2} \left(m_A^2 \sin 2\beta - 2\frac{\kappa}{\lambda} \mu^2 \right) \sin 2\beta + \frac{\kappa}{\lambda} \mu \left(A_\kappa + 4\frac{\kappa}{\lambda} \mu \right). \quad (2.11)$$

Note that the combination $\frac{\kappa}{\lambda} \mu A_\kappa$, that appear in m_S^2 , also appeared in $m_{A_s}^2$ [see Eq. (2.4)]. While $\frac{\kappa}{\lambda} \mu A_\kappa$ could not be too large and positive in order for $m_{A_s}^2$ to be positive, we see that it also can not be too large and negative in order for m_S^2 to be positive. This term also introduces certain correlation between μ and A_κ , as discussed in Secs. 4 and 5. For large m_A , we see that $m_{H_v}^2$ grows with m_A , while m_{h_v} remains around the electroweak scale. The singlet, on the other hand, is determined by a combination of μ , A_κ , and m_A , as well as the dimensionless quantities κ , λ , and $\tan \beta$.

The first and foremost effect of the introduction of the singlet and its couplings to the MSSM Higgs sector is the extra λ -term in Eqs. (2.9) and (2.10), which lifts up the mass of the SM-like Higgs $m_{h_v}^2$, in particular, for small $\tan \beta$, while reducing $m_{H_v}^2$. In the MSSM, for the SM-like Higgs to have a mass of approximately 126 GeV typically requires the tree-level Higgs mass-squared $m_Z^2 \cos^2 2\beta$ to be maximized, which prefers large $\tan \beta$. In the NMSSM, by contrast, the contribution from $\frac{1}{2}(\lambda v)^2 \sin^2 2\beta$ results in small values of $\tan \beta$ being favored, especially for large λ . Consequently, the contribution to the Higgs mass from stop sector loop corrections can be relaxed. The left-right mixing in the stop sector is no longer required to be near maximal ($|A_t| \sim \sqrt{6M_{3SQ}M_{3SU}}$ in the MSSM).

The mixture of the singlet with the MSSM Higgs sector, in particular with h_v , could further affect the SM-like Higgs mass. If we consider only the h_v - S mixing for simplicity, when $m_{h_v}^2 > m_S^2$, the mass eigenvalues for the SM-like Higgs is pushed up after the diagonalization of the 2×2 mass matrix. This is the so-called ‘‘push-up’’ scenario described in

the literature. On the other hand, when $m_{h_v}^2 < m_S^2$, the mass eigenvalue for the SM-like Higgs is pushed down due to the mixing, and is, thus, called the “push-down” scenario. Such effects have been discussed extensively in the literature [11, 19], considered almost exclusively in the limit of $m_A \gg m_Z$, which decouples the effect of the MSSM non-SM like Higgs H_v , while focusing only on the mixture of h_v and S . The low-lying spectrum in such cases includes two CP-even Higgs bosons, H_1 and H_2 , as a mixture of h_v and S , with either H_1 or H_2 being the 126 GeV SM-like Higgs, corresponding to the push-down or push-up scenario, respectively. In this large- m_A scenario, only one CP-odd Higgs A_s might be light, while A_v and H^\pm are heavy and decouple. Both the push-up and push-down scenarios, however, suffer from a certain degree of fine-tuning for the NMSSM parameters if the stop masses are relatively light and the left-right mixing in the stop sector is not large [11].

2.2 Low- m_A Region

In this paper, we consider the region of the NMSSM with relatively small m_A ($m_A \lesssim 2m_Z$). In this region, all the MSSM-type Higgs bosons are relatively light, with $m_{h_v}^2$ and $m_{H_v}^2$ relatively close to each other. With an appropriate choice of other NMSSM parameters, m_S^2 and $m_{A_s}^2$ can be light as well. This could lead to potentially large mixing effects in the Higgs mass eigenstates, resulting in possible deviations of the SM-like Higgs couplings to the gauge boson and fermion sectors.

The low- m_A region of the MSSM (the so-called “non-decoupling” region) has been studied in Refs. [16, 35–40]. It was pointed out that for $m_A \sim m_Z$, the heavy CP-even Higgs, H^0 in the usual MSSM notation, is the SM-like Higgs. On the other hand, for the light CP-even Higgs h^0 to be SM-like, m_A is typically large: $m_A \gtrsim 300$ GeV, in the so-called “decoupling” region of the MSSM. However, these observations do not necessarily hold in the NMSSM, due to the singlet-induced λ -term contribution to $m_{h_v}^2$ and $m_{H_v}^2$, as well as the singlet mixing effects in the mass matrix.

If we ignore the singlet mixture with h_v and H_v for the moment, and study the consequence of the extra λ -term in the 2×2 (h_v, H_v) system in the NMSSM, then, to have the heavy CP-even MSSM Higgs be SM-like, $m_{h_v}^2 \geq m_{H_v}^2$, requires

$$m_A^2 \leq m_Z^2 \cos 4\beta + (\lambda v)^2 \sin^2 2\beta. \quad (2.12)$$

Fig. 2 shows the lines in the λ versus m_A plane when $m_{h_v}^2 = m_{H_v}^2$, for various values of $\tan \beta$. For regions above the lines, $m_{h_v}^2 > m_{H_v}^2$, and the heavy CP-even MSSM Higgs is SM-like (up to mixing and loop corrections). For regions below the lines, $m_{h_v}^2 < m_{H_v}^2$, and the light CP-even MSSM Higgs is SM-like. All the lines cross the point $m_A = m_Z$ and $\lambda = \sqrt{2}m_Z/v \sim 0.5$. For small $\tan \beta \sim 1$, large λ (above the $\tan \beta = 1$ line) is preferred to realize $m_{h_v} > m_{H_v}$, while small λ gives rise to $m_{h_v} < m_{H_v}$. For larger values of $\tan \beta$, the curve tilts more and more vertically. For $\tan \beta \gtrsim 10$, the λ dependence becomes rather weak and the separation of the two regions is governed by the value of m_A : $m_A \lesssim m_Z$ for $m_{h_v} > m_{H_v}$ and $m_A \gtrsim m_Z$ for $m_{h_v} < m_{H_v}$, which is similar to the usual MSSM case. In Fig. 2, we also include the m_{H^\pm} contours as dashed lines, with the shaded area indicating the region ruled out by $m_{H^\pm}^2 < 0$. Taking into account the LEP bound of

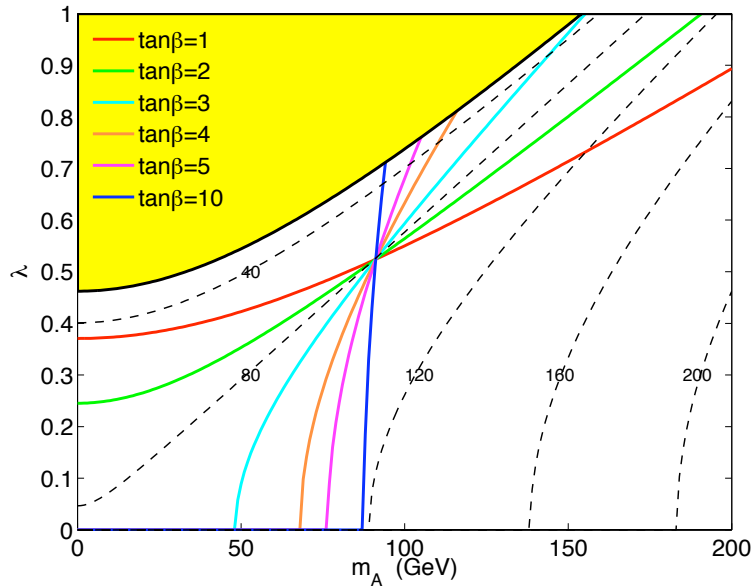


Figure 2. Lines for $m_{h_v}^2 = m_{H_v}^2$ for different values of $\tan\beta$ in the λ versus m_A plane. $m_{h_v}^2 > m_{H_v}^2$ above the lines and $m_{h_v}^2 < m_{H_v}^2$ below the lines. Also shown by the dashed lines are the mass contours for the tree-level value of m_{H^\pm} . The shaded region corresponds to the excluded region with $m_{H^\pm}^2 < 0$.

$m_{H^\pm} \gtrsim 80$ GeV [33, 34] limits us to the right of the $m_{H^\pm} = 80$ GeV contour. Therefore, requiring $m_{h_v} > m_{H_v}$ while satisfying the experimental charged Higgs bounds restricts us to two regions: large $\lambda \gtrsim 0.5$, $m_A \gtrsim m_Z$ for small $\tan\beta \sim 1-2$, or small $\lambda \lesssim 0.5$, $m_A \lesssim m_Z$ for $\tan\beta \gtrsim 2$. Imposing a stronger bound on m_{H^\pm} from $t \rightarrow bH^\pm$ searches at the Tevatron and the LHC [41–43] further narrows down the $m_{h_v} > m_{H_v}$ region, resulting in a fine-tuned region to realize.

On the other hand, $m_{h_v} < m_{H_v}$ is much easier to realize in the NMSSM. In contrast to the MSSM, where being deep into the decoupling region $m_A \gtrsim 300$ GeV is typically required to satisfy both the mass window and the cross section requirement (i.e. for h^0 to obtain SM-like couplings to the gauge bosons), in the NMSSM, with the mixture of the singlet and the possible suppressed couplings to $b\bar{b}$, even a suppressed coupling to the gauge sector could be accommodated while satisfying the experimentally observed cross section range. Note that our discussions are based on tree level expression for the Higgs masses. While including loop corrections shifts all the masses, our statements are still qualitatively valid.

Including the extra singlet in the spectrum gives three distinct cases, as sketched in Fig. 1, corresponding to either H_1 , H_2 , or H_3 being SM-like:

- H_1 SM-like: $m_{h_v} \lesssim m_{H_v}, m_S$,
- H_2 SM-like: $m_S \lesssim m_{h_v} \lesssim m_{H_v}$ or $m_{H_v} \lesssim m_{h_v} \lesssim m_S$,
- H_3 SM-like: $m_{H_v}, m_S \lesssim m_{h_v}$.

	H_i	A_i		H^\pm
R_{uu}	$\xi_{H_i}^{h_v} + \xi_{H_i}^{H_v} / \tan \beta$	$\xi_{A_i}^{A_v} / \tan \beta$	$R_{d_L u_R^c}$	$-1 / \tan \beta$
R_{dd}	$\xi_{H_i}^{h_v} - \xi_{H_i}^{H_v} \tan \beta$	$\xi_{A_i}^{A_v} \tan \beta$	$R_{u_L d_R^c}$	$-\tan \beta$
R_{VV}	$\xi_{H_i}^{h_v}$			

Table 1. Reduced Higgs couplings at tree level. The charged Higgs couplings of $H^+ d_L u_R^c$ and $H^- u_L d_R^c$ are normalized to the SM top and bottom Yukawa couplings $\sqrt{2}m_t/v$ and $\sqrt{2}m_b/v$, respectively.

With the off-diagonal mixing in the mass matrix, the separation of these regions becomes less distinct while the above relations still approximately hold.

2.3 Couplings

The mass eigenstates $H_{1,2,3}$ are, in general, a mixture of h_v , H_v , and S :

$$H_i = \sum_{\alpha} \xi_{H_i}^{H_{\alpha}} H_{\alpha}, \quad \text{for } i = 1, 2, 3, \quad H_{\alpha} = (h_v, H_v, S), \quad (2.13)$$

with $\xi_{H_i}^{H_{\alpha}}$ being the 3×3 unitary matrix that rotates the Higgs bosons into the mass eigenstates. In particular, $|\xi_{H_i}^{H_{\alpha}}|^2$ defines the fraction of h_v , H_v , and S in H_i with the unitarity relations:

$$|\xi_{H_1}^{H_{\alpha}}|^2 + |\xi_{H_2}^{H_{\alpha}}|^2 + |\xi_{H_3}^{H_{\alpha}}|^2 = 1, \quad |\xi_{H_i}^{h_v}|^2 + |\xi_{H_i}^{H_v}|^2 + |\xi_{H_i}^S|^2 = 1. \quad (2.14)$$

Similarly, for the CP-odd Higgs bosons, the unitary rotation is $A_i = \sum_{\alpha} \xi_{A_i}^{A_{\alpha}} A_{\alpha}$ where $i = 1, 2$, and $A_{\alpha} = (A_v, A_s)$. The fractions of A_v and A_s in the CP-odd mass eigenstates $A_{1,2}$ are given by $|\xi_{A_i}^{A_{\alpha}}|^2$, $i = 1, 2$, with $|\xi_{A_1}^{A_v}|^2 = |\xi_{A_2}^{A_s}|^2 = 1 - |\xi_{A_1}^{A_s}|^2 = 1 - |\xi_{A_2}^{A_v}|^2$.

In Table 1, we express the tree-level reduced couplings of the NMSSM Higgs mass eigenstates to various pairs of SM particles, which are the ratios of the NMSSM Higgs couplings to the corresponding SM values. The charged Higgs couplings of $H^+ d_L u_R^c$ and $H^- u_L d_R^c$ are normalized to the SM top and bottom Yukawa couplings $\sqrt{2}m_t/v$ and $\sqrt{2}m_b/v$, respectively. In the NMSSM, the $H_i ZZ$ and $H_i WW$ couplings are always modified in the same way at leading order. Therefore, we use VV to represent both WW and ZZ . The coupling of the CP-even Higgs bosons to the gauge boson sector VV is completely determined by the h_v -fraction of H_i : $|\xi_{H_i}^{h_v}|^2$, which plays an important role in understanding the coupling and branching fraction behavior of the SM-like Higgs boson. Note that $|\xi_{H_i}^{h_v}|^2 \leq 1$, therefore, the $H_i VV$ couplings, as well as the $H_i \rightarrow VV$ partial decay widths, are always suppressed compared to their SM values. However, the branching fractions of $H_i \rightarrow VV$ could still be similar or even enhanced compared to their SM values, since $H_i \rightarrow bb$ could be suppressed as well.

The Higgs to $\gamma\gamma$ and Higgs to gg couplings are both loop-induced. The dominant contribution to the $h_v \gamma\gamma$ coupling comes from the WW loop, with a sub-leading destructive contribution from the top loop. The $h_v gg$ coupling, on the other hand, is dominated by the top-loop contribution. The $H_i \gamma\gamma$ and $H_i gg$ couplings are modified similarly in the NMSSM, based on the reduced couplings as listed in Table 1.

3 Parameter Scan and Constrained Regions

We will focus our scan on the parameters that are most relevant to the Higgs sector, namely, parameters appearing in the Higgs potential, as well as the stop mass parameters, which could induce a relatively large loop correction to the Higgs mass. Since the impact of other SUSY sectors to the Higgs mass is typically small, we effectively decouple them by setting all other SUSY mass parameters to be 3 TeV and the other trilinear soft SUSY breaking parameters to be 0. Note that the sbottom and stau might modify the Higgs mass and certain couplings at loop level, which could have substantial effects in certain regions of parameter space. We defer a discussion of these regions to specific studies in the literature [44] and will only focus on the Higgs and stop sectors in the current study.

In the MSSM, the relevant Higgs and stop sector parameters are

$$m_A, \tan\beta, \mu, M_{3SQ}, M_{3SU}, A_t, \quad (3.1)$$

as well as the Higgs vacuum expectation value $v = 246$ GeV. In the NMSSM, the tree level Higgs potential involves seven parameters: $(\lambda, \kappa, A_\lambda, A_\kappa, v_s, \tan\beta)$ and v . After replacing v_s by $\mu = \lambda v_s/\sqrt{2}$ and replacing A_λ by m_A as defined in Eq. (2.4), we are left with three new parameters compared to the MSSM case. We scan these parameters in the range of

$$\begin{aligned} 0 &\leq m_A &\leq 200 \text{ GeV}, \\ 1 &\leq \tan\beta &\leq 10, \\ 100 \text{ GeV} &\leq \mu &\leq 1000 \text{ GeV}, \\ 0.01 &\leq \lambda, \kappa &\leq 1, \\ -1200 \text{ GeV} &\leq A_\kappa &\leq 200 \text{ GeV}, \\ 100 \text{ GeV} &\leq M_{3SQ}, M_{3SU} &\leq 3000 \text{ GeV}, \\ -4000 \text{ GeV} &\leq A_t &\leq 4000 \text{ GeV}, \end{aligned} \quad (3.2)$$

unless otherwise stated. The range of m_A is chosen to guarantee that H_v and A_v are light. The ranges of μ , λ , κ and A_κ are chosen such that the CP-even and odd singlet masses are allowed to vary over a wide range. The stop sector mass and mixing parameters are chosen to cover both the minimal and maximal mixing scenarios. We restrict $\tan\beta$ to be in the range of 1 – 10 since regions with higher values of $\tan\beta$ do not contain a SM-like Higgs boson in the mass window of 124 – 128 GeV, as will be discussed in detail in Secs. 4 and 5.

The scan is performed by utilizing NMSSMTools 3.2.1 [45–47] to calculate the Higgs and SUSY spectrum, Higgs couplings, decay widths, branching fractions, and various Higgs production cross sections. The full constraints imposed for the scan procedure include:

- the latest LHC limits in various SM Higgs searches [48–54];
- bounds on MSSM Higgs search channels from LEP, the Tevatron, and the LHC [14, 55];
- stop and sbottom masses to be heavier than 100 GeV.

We did not impose bounds that are not directly relevant to the Higgs sector, for example, other SUSY particle searches, flavor physics, and dark matter relic density. Those bounds typically involve SUSY parameters of other NMSSM sectors which we did not scan. Although some significant reduction of the allowed parameter space may occur with these additional constraints, we do not expect our conclusions to be changed. We generated a large Monte Carlo sample over the multi-dimensional parameter space and tested each parameter point against the experimental constraints. For the following presentation, the allowed points (or regions) in the plots are indicative of consistent theoretical solutions satisfying the experimental constraints, but are not meant to span the complete space of possible solutions.

Given the discovery of a SM-like Higgs boson around 126 GeV, we study its implication by applying the following requirements step by step:

$$\text{Either } H_1, \text{ or } H_2, \text{ or } H_3 \text{ in the mass window of } 124 - 128 \text{ GeV}, \quad (3.3)$$

$$\frac{\sigma \times \text{Br}(gg \rightarrow H_i \rightarrow \gamma\gamma)}{(\sigma \times \text{Br})_{\text{SM}}} \geq 0.8, \quad \frac{\sigma \times \text{Br}(gg \rightarrow H_i \rightarrow WW/ZZ)}{(\sigma \times \text{Br})_{\text{SM}}} \geq 0.4. \quad (3.4)$$

The cases delineated in Eqs. (3.3) and (3.3) determine the defining feature of the regions described in this paper and will, henceforth, be referred to as H_1 -126, H_2 -126 and H_3 -126, respectively.

Figure 3 shows the allowed mass regions versus m_{H^\pm} for the CP-even Higgs bosons (left panels) and the CP-odd/charged Higgs bosons (right panels). The first and second row panels are for points that pass all the experimental constraints as itemized earlier, as well as H_1 and H_2 , respectively, satisfying both the mass and cross section requirements as listed in Eqs. (3.3) and (3.4). The third row panels are for points that pass all experimental constraints as well as H_3 satisfying the mass requirement as listed in Eq. (3.3). We have chosen to plot the physical Higgs masses against the charged Higgs mass m_{H^\pm} , rather than the conventional choice of m_A as in the MSSM. Due to the relatively large loop corrections to the Higgs masses, the natural scale parameter choice in the NMSSM would be the loop corrected A_v mass $m_{A_{loop}}$, the NMSSM equivalent of the MSSM m_A (the physical mass for the CP-odd MSSM Higgs). A_v , however, has to mix with A_s to provide masses for the two CP-odd mass eigenstates A_1 and A_2 . The charged Higgs mass m_{H^\pm} , on the other hand, retains roughly the simple relationship with $m_{A_{loop}}$, described in Eq. (2.6), after loop corrections. Therefore, we choose the physical m_{H^\pm} as the scale parameter in Fig. 3. In this figure, we scanned in the range $0 \text{ GeV} < m_{H^\pm}^{\text{tree}} < 300 \text{ GeV}$, rather than $0 \text{ GeV} < m_A < 200 \text{ GeV}$, to improve the coverage of the parameter region of our interest.

For H_1 being the SM-like Higgs in the mass window of 124 – 128 GeV (see the first row of Fig. 3), H_2 is typically in the mass range of 125 – 300 GeV, while $m_{H_3} \gtrsim 200 \text{ GeV}$. The charged Higgs mass is in the approximate range 125 – 300 GeV. Charged Higgs bosons with mass less than 150 GeV are mostly ruled out by the direct search for H^\pm produced in top decays. The light CP-odd Higgs could be very light, a few GeV $\lesssim m_{A_1} \lesssim 300 \text{ GeV}$, while $m_{A_2} \gtrsim 200 \text{ GeV}$. When $m_{A_1} < m_{H_1}/2$, the decay channel $H_1 \rightarrow A_1 A_1$ opens, leading to very interesting phenomenology, as will be discussed in detail in Sec. 4. Note that the

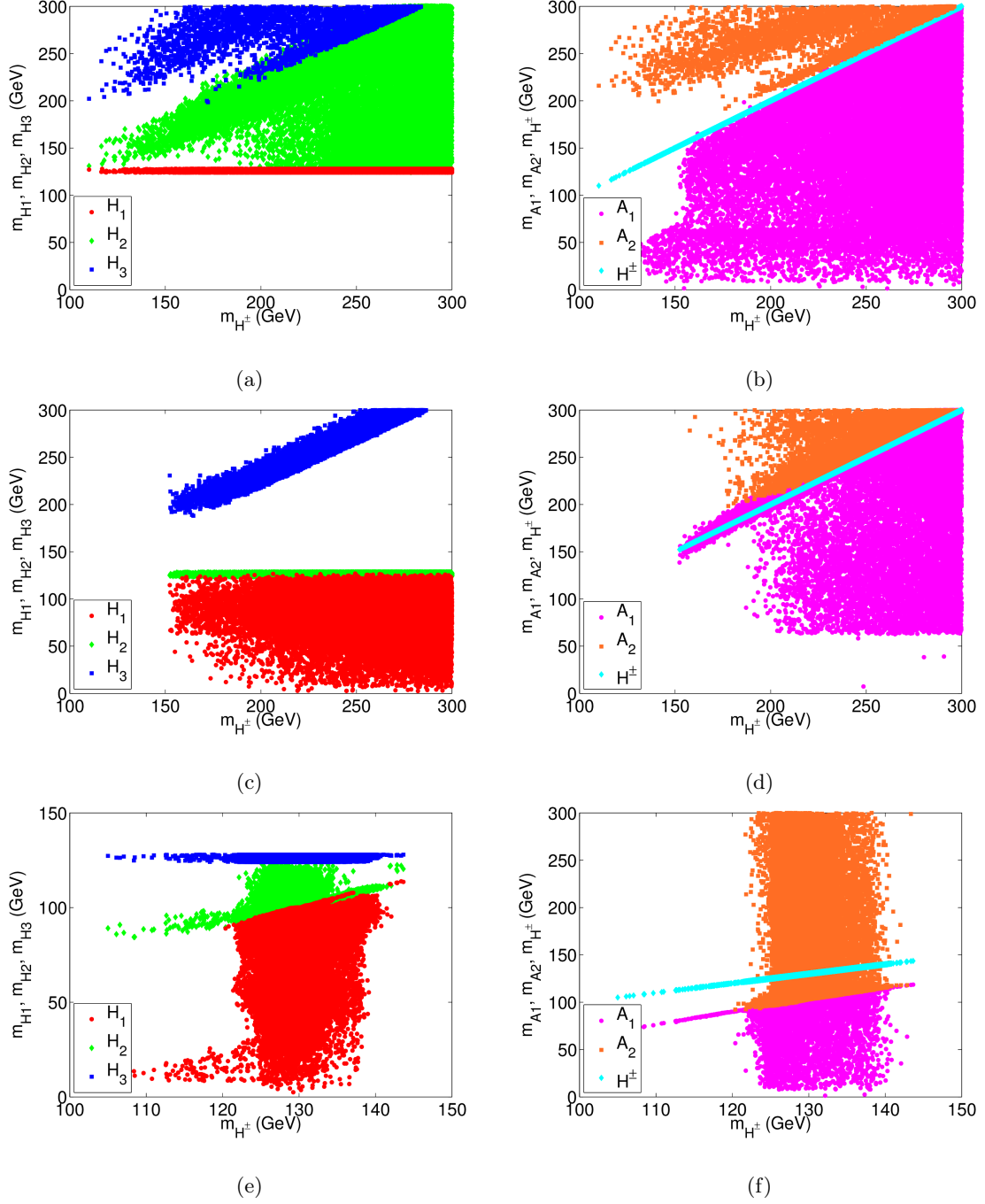


Figure 3. The left panels show the allowed mass regions versus m_{H^\pm} for the CP-even H_1 (red), H_2 (green), and H_3 (blue). The right panels show the allowed mass regions versus m_{H^\pm} for the CP-odd A_1 (magenta), and A_2 (brown), as well as the charged Higgs H^\pm (cyan). The first and second row panels contain the points that pass all the experimental constraints as well as having H_1 and H_2 , respectively, satisfying both the mass and cross section requirements as listed in Eqs. (3.3) and (3.4). The third row panels contain the points that pass all the experimental constraints as well as Eq. (3.3), but not Eq. (3.4).

boundary of the H_2 and H_3 regions, as well as the boundary of the A_1 and A_2 regions show nice correlation with m_{H^\pm} . This is because the boundary is given by m_{H_v} as in Eq. (2.10) for the CP-even case, and by m_A for the CP-odd case, both of which scale with m_{H^\pm} . The singlet mixing with H_v and A_v will push/pull the mass eigenstates away from m_{H_v} and m_A , leaving a clear boundary. Given a H_2, H_3 pair (A_1, A_2 pair), the one whose mass is closer to the H_2 - H_3 (A_1 - A_2) boundary line is more H_v (A_v)-like.

For H_2 being the SM-like Higgs in the mass window of 124 – 128 GeV (see the second row of Fig. 3), a large fraction of the points contain H_1 in the mass range of 60 – 124 GeV. There is also a significant set of points with $m_{H_1} < m_{H_2}/2$, which turns on the decay channel $H_2 \rightarrow H_1 H_1$, as will be discussed in Sec. 5. m_{H_3} is in the mass window of approximately 200–350 GeV, and grows roughly linearly with m_{H^\pm} , an indication of H_3 being mostly H_v -like. The points with m_{H_3} below ~ 180 GeV are removed by a combination of the collider constraints and the cross section requirement of Eq. (3.4). This is very different from the H_1 -126 case, in which H_3 could be singlet dominant with mass as large as 1 TeV or higher. For the light CP-odd Higgs A_1 , it falls into two regions: one region with 60 GeV $\lesssim m_{A_1} \lesssim 300$ GeV ($m_{H^\pm} \gtrsim 200$ GeV), with little dependence on m_{H^\pm} (for A_1 being mostly A_s); another region with $m_{A_1} \gtrsim 150$ GeV ($m_{H^\pm} \gtrsim 150$ GeV), which grows linearly with m_{H^\pm} (for A_1 being A_v -like). A_2 typically has a mass of 200 GeV or higher, which also falls into two regions accordingly.

For H_3 being the SM-like Higgs in the mass window of 124 – 128 GeV (see the third row of Fig. 3), both the singlet and H_v -dominant Higgs bosons need to be lighter than about 126 GeV. Given the tight experimental constraints on the light Higgs searches, as well as the fine-tuning between the mass parameters, this region turns out to be highly restrictive. While we can realize regions with m_{H_3} in the desired mass window, it is extremely difficult to satisfy the cross section requirement of Eq. (3.4). Panels in the third row of Fig. 3 show points with H_3 in the mass window of 124 – 128 GeV. However, $\sigma \times \text{Br}(gg \rightarrow H_3 \rightarrow \gamma\gamma, WW/ZZ)/\text{SM}$ is less than 0.4 in general, and it is therefore hard to accommodate the observed Higgs signal as H_3 in the NMSSM.

In what follows, we will discuss the H_1 -126 and H_2 -126 cases in detail, exploring the relevant parameter space for each region, the composition of the 126 GeV SM-like Higgs and the other light NMSSM Higgs bosons, possible enhancement or suppression of various search channels as well as correlations between them.

4 H_1 as the SM-like Higgs Boson

4.1 Parameter Regions

For H_1 to have SM-like cross sections for $gg \rightarrow H_1 \rightarrow \gamma\gamma, WW/ZZ$ within the experimentally observed ranges, H_1 needs to be either dominantly h_v or have a considerable singlet fraction with a suppressed $H_1 \rightarrow b\bar{b}$ partial width. H_v and S dominant states are typically heavier such that, usually, the lightest CP-even Higgs state is mostly h_v . This case is seldom realized in the MSSM low- m_A region ($m_A \lesssim 2m_Z$), since the light CP-even Higgs boson typically has suppressed couplings to WW and ZZ in this region. In the NMSSM, the tree-level diagonal mass term for h_v is $m_{h_v}^2 = m_Z^2 \cos^2 2\beta + \frac{1}{2}(\lambda v)^2 \sin^2 2\beta$. Large λ and

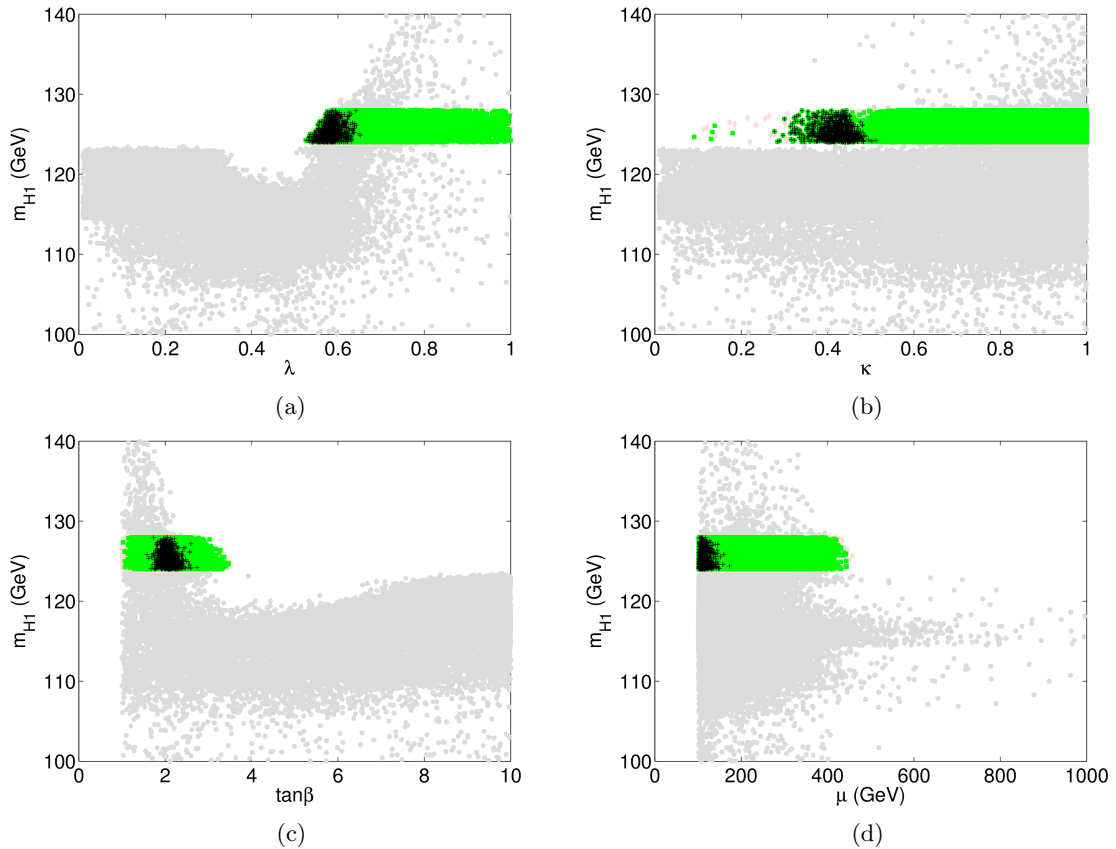


Figure 4. The dependence of m_{H_1} on the following NMSSM parameters in the H_1 -126 case: λ , κ , $\tan\beta$, and μ . Grey points are those that pass the experimental constraints, pale-pink points are those with H_1 in the mass window $124 \text{ GeV} < m_{H_1} < 128 \text{ GeV}$ and green points are those with the cross section requirements further imposed. Black points are those that remain perturbative up to the Planck scale.

small $\tan\beta$ are preferred to push up the mass of h_v into the desired mass window. For small $\tan\beta$, even for small m_A , typically $m_{h_v}^2 < m_{H_v}^2$, resulting in the lighter MSSM-like CP-even Higgs being SM-like in the low- m_A region. In addition, mixture with the singlet in the NMSSM which produces, in particular, a suppressed $H_1 \rightarrow b\bar{b}$ partial decay width, could lead to a SM-like $\gamma\gamma$ and WW/ZZ branching fraction for H_1 as well. The push-down effect in mass eigenvalues from the singlet mixing also helps to realize the mostly h_v state being H_1 .

To show the effect of the narrowing down of the parameter regions due to the mass and cross section requirements, Fig. 4 presents the dependence of m_{H_1} on λ , κ , $\tan\beta$, and μ , with gray dots for all points satisfying the experimental constraints, pale-pink points which pass the mass window requirement of Eq. (3.3), and green points, that almost overlap the pale-pink points, which pass both the mass and cross section requirements of Eqs. (3.3) and (3.4).

After requiring H_1 to fall into the mass region of $124 - 128 \text{ GeV}$, we are restricted to the parameter region of $\lambda \gtrsim 0.55$, $\kappa \gtrsim 0.3$ (with a small number of points down to

	$\tan\beta$	m_A (GeV)	μ (GeV)	λ	κ	A_λ (GeV)	A_κ (GeV)
H_1 -126	1~3.5	0~200	100~500	$\gtrsim 0.55$	$\gtrsim 0.3$	-650~300	-1200~200
perturb.	1.5 ~2.5	150~200	100~150	0.55~0.65	0.3~0.5	-30~230	-150~100
$m_{A_1} < \frac{m_{H_1}}{2}$	1~3.5	100~200	100~200	$\gtrsim 0.55$	$\gtrsim 0.5$	-150~150	-50~30

Table 2. NMSSM Parameter regions for the H_1 -126 case.

0.1), $1 \lesssim \tan\beta \lesssim 3.5$, $\mu \lesssim 500$ GeV, -1200 GeV $\lesssim A_\kappa \lesssim 200$ GeV with no restriction on m_A which is allowed to be in the entire region of $0 - 200$ GeV (the corresponding region for A_λ is approximately -650 GeV to 300 GeV). The stop mass parameters M_{3SQ} , M_{3SU} and A_t are unrestricted as well. Further imposing the cross section requirement for $gg \rightarrow H_1 \rightarrow \gamma\gamma, WW$ and ZZ does not narrow down the allowed regions for these parameters further.

Also shown as the black points in Fig. 4 are the parameter points where λ and κ remain perturbative up to the Grand Unified Theory (GUT) scale. They occupy a small region of $0.5 \lesssim \lambda \lesssim 0.65$, $0.3 \lesssim \kappa \lesssim 0.5$, $\tan\beta \sim 2$, $100 \lesssim \mu \lesssim 150$ GeV, $-150 \lesssim A_\kappa \lesssim 100$ GeV, and $150 \lesssim m_A \lesssim 200$ GeV ($-30 \lesssim A_\lambda \lesssim 230$ GeV). While M_{3SQ} and M_{3SU} are unconstrained, $|A_t|$ is restricted to be $\gtrsim 1200$ GeV. These parameter regions are summarized in Table 2.

We have noted earlier that the light CP-odd Higgs A_1 could be very light. When it falls below half of the H_1 mass, $H_1 \rightarrow A_1 A_1$ opens up, which could dominate the H_1 decay width, compared to the usual case in which decay to $b\bar{b}$ dominates. Therefore, we further separate the H_1 -126 case into three regions:

- H_1 Region IA: $m_{A_1} > m_{H_1}/2$ and $|\xi_{H_1}^{h\nu}|^2 > 0.7$: green points in Figs. 5-10.
- H_1 Region IB: $m_{A_1} > m_{H_1}/2$ and $|\xi_{H_1}^{h\nu}|^2 < 0.7$: red points in Figs. 5-10.
- H_1 Region II: $m_{A_1} < m_{H_1}/2$: magenta points in Figs. 5-10.

To identify the NMSSM parameter regions that give a SM-like H_1 in the mass window of $124 - 128$ GeV, in Fig. 5, we show the viable regions in various combinations of NMSSM parameters. Grey points are those that pass the experimental constraints, pale-pink points are those with H_1 in the mass window 124 GeV $< m_{H_1} < 128$ GeV, green and red points are for H_1 Region I with m_{A_1} above the $H_1 \rightarrow A_1 A_1$ threshold, and magenta points are for H_1 Region II with low m_{A_1} . Again, the black points are those where λ and κ remain perturbative up to the GUT scale.

The first two panels show the (a) λ versus m_A , and (b) κ versus m_A regions. For small values of m_A , λ has to be around $0.6-0.7$, since too large a value of λ is ruled out by the charged Higgs mass bounds, while too small a value of λ results in m_{H_1} being less than 124 GeV. For larger values of m_A , the λ range is enlarged to $0.55 \lesssim \lambda \lesssim 1$. κ , on the other hand, has to be ~ 1 for small m_A , while smaller κ is allowed for larger m_A .

Panel (c) of Fig. 5 shows the viable region in the λ versus κ plane. Given $\lambda \gtrsim 0.55$ and $\kappa \gtrsim 0.3$, the renormalization group running of λ , and κ , as well as of the Yukawa

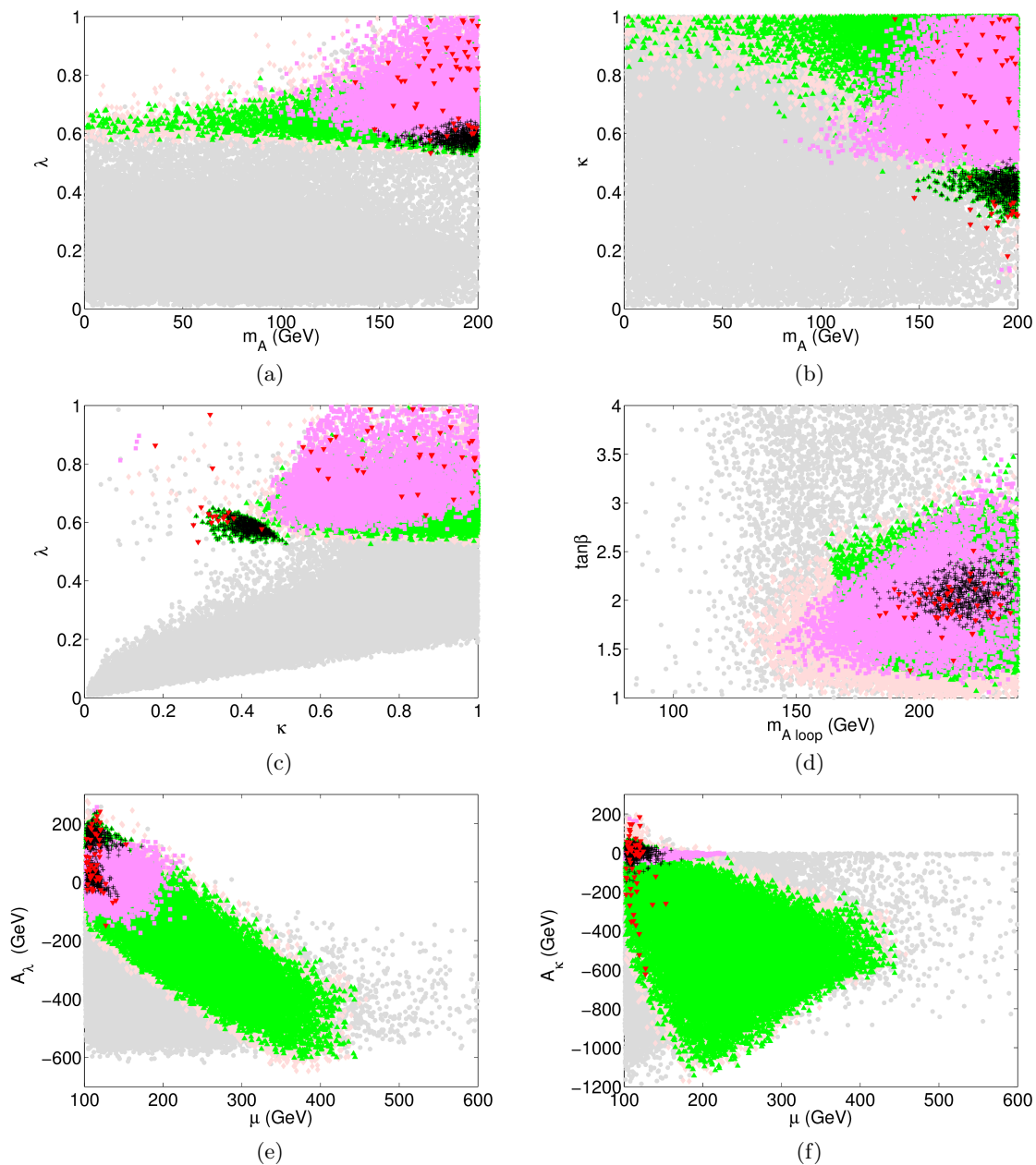


Figure 5. Viable NMSSM parameter regions in the H_1 -126 case: (a) λ versus m_A , (b) κ versus m_A , (c) λ versus κ , (d) $\tan\beta$ versus $m_{A_{loop}}$, (e) A_λ versus μ , and (f) A_κ versus μ . Grey points are those that pass the experimental constraints, pale-pink points are those with H_1 in the mass window $124 \text{ GeV} < m_{H_1} < 128 \text{ GeV}$. Green points are for H_1 Region IA: $m_{A_1} > m_{H_1}/2$ and $|\xi_{H_1}^{h\nu}|^2 > 0.7$. Red points are for H_1 Region IA: $m_{A_1} > m_{H_1}/2$ and $|\xi_{H_1}^{h\nu}|^2 < 0.7$. Magenta points are for H_1 Region II: $m_{A_1} < m_{H_1}/2$. The black points are those where λ and κ remain perturbative up to the GUT scale.

couplings $y_{t,b}$ and gauge couplings might reach the Landau pole before M_{GUT} . As noted in Ref. [6], a larger λ allows a highly natural light Higgs boson. For all the points that pass

the mass and cross section requirements, only a small region of the λ - κ plane, as shown by the black points in panel (c) of Fig. 5, remain perturbative up to the GUT scale around 10^{16} GeV. For larger values of κ , it reaches the Landau pole before the other couplings. While the running of λ is much slower, it has a large impact on the running of the gauge couplings and Yukawa couplings. Increasing the value of λ would accelerate the running of the top Yukawa coupling. However, for all the viable points that pass both the mass and cross section requirements, the scale at which at least one of the couplings becomes non-perturbative is typically larger than 10^7 GeV, much higher than the electroweak scale. Since adding new multiplets or other new physics could affect the running of the couplings and delay the Landau pole scale, in our study, we relax the perturbativity constraint and only place a loose upper bound of $\lambda, \kappa \leq 1$. All of our parameter points remain perturbative up to at least the scale of 10^7 GeV.

Panel (d) of Fig. 5 shows the viable region in the $\tan\beta$ - $m_{A_{loop}}$ plane, where we have plotted $m_{A_{loop}}$ for better comparison with the MSSM.¹ Unlike in the MSSM case, where constraints from collider direct Higgs searches and the light CP-even Higgs h^0 being SM-like require the parameters to be in the decoupling region of $m_A \gtrsim 300$ GeV [16], in the NMSSM, by contrast, with the push-down effect from the singlet mixing and the extra contribution from $\frac{1}{2}(\lambda v)^2 \sin^2 2\beta$ to the tree level mass squared for h_v , H_1 could be the SM-like Higgs in the low- m_A region: $m_{A_{loop}} \gtrsim 140$ GeV (while the tree-level m_A could be as low as a few GeV). The range of $\tan\beta$ is smaller compared to that of the MSSM:² $1 \lesssim \tan\beta \lesssim 3$, since smaller $\tan\beta$ is preferred for providing a sizable contribution from the λ -term to the tree level Higgs mass $m_{h_v}^2$.

Panel (e) of Fig. 5 shows a clear correlation between A_λ and μ . This is because a larger value of μ is needed to cancel the negative contribution from A_λ to keep $m_A^2 > 0$, as given in Eq. (2.4). Panel (f) of Fig. 5 shows a weaker correlation between A_κ and μ . While larger μ is typically preferred for a larger negative A_κ , μ can not be too large since otherwise at least one of the CP-even Higgs masses squared becomes negative.

The magenta points in Fig. 5 are in H_1 Region II: $m_{A_1} < m_{H_1}/2$. It maps out the region of small $|A_\kappa|$, $|A_\lambda|$ and μ : $-50 \lesssim A_\kappa \lesssim 30$ GeV, $-150 \lesssim A_\lambda \lesssim 150$ GeV, $100 \lesssim \mu \lesssim 200$ GeV. m_A is restricted to be in the range of $100 - 200$ GeV ($m_{A_{loop}} \gtrsim 150$ GeV), and κ in the range of $0.5 - 1$. Ranges for λ and $\tan\beta$, however, are not narrowed compared to the generic H_1 Region I, as shown as the green points in Fig. 5.

Unlike in the MSSM case, where the mass parameters for the stop sector, M_{3SQ} and M_{3SU} , are correlated with the stop left-right mixing A_t to be close to the m_h^{max} scenario, $|A_t| \sim \sqrt{6M_{3SQ}M_{3SU}}$, there is no obvious correlation between M_{3SQ} , M_{3SU} , and A_t in the NMSSM. All the ranges are allowed for these parameters. This is because in the MSSM, we need large loop corrections to the Higgs mass from the stop sector to push it to the $124 - 128$ GeV mass window, which requires either large stop masses around $5 - 10$ TeV or large stop mixing. In the NMSSM, such a lift to the Higgs mass could be achieved by the $(\lambda v)^2$ contribution to the Higgs mass at tree level, resulting in a less constrained stop

¹ m_A in the MSSM is the physical mass for the CP-odd Higgs A^0 , with loop corrections already included.

² $\tan\beta \leq 3$ is excluded by the LEP Higgs searches in the MSSM [60].

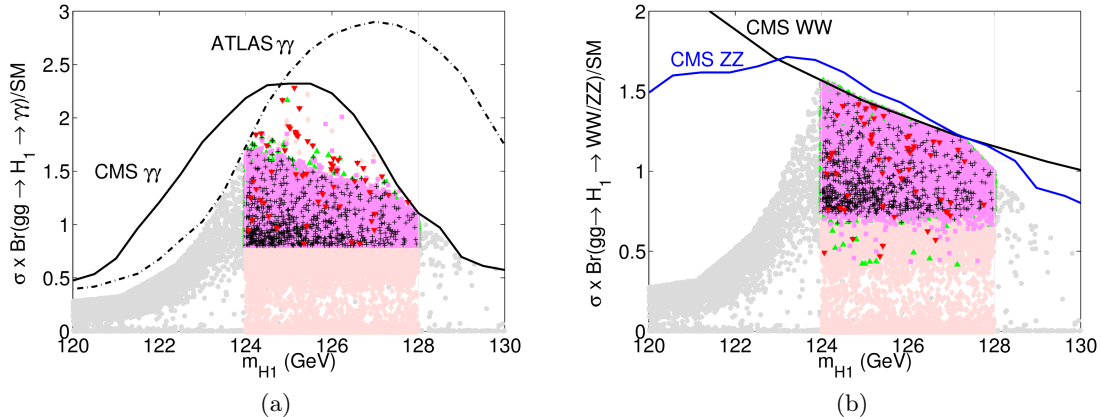


Figure 6. The normalized $\sigma \times \text{Br}/\text{SM}$ for (a) $gg \rightarrow H_1 \rightarrow \gamma\gamma$ and (b) $gg \rightarrow H_1 \rightarrow WW/ZZ$ as a function of m_{H_1} in the H_1 -126 case. The current experimental constraints from the SM Higgs searches of the $\gamma\gamma$, WW and ZZ channels are also imposed. Color coding is the same as for Fig. 5.

sector. The mass for the lightest stop can be as light as 100 – 200 GeV, with slightly larger mass splitting $\Delta m_{\tilde{t}} \gtrsim 200 - 300$ GeV anticipated for small $m_{\tilde{t}_1}$. However, once $m_{\tilde{t}_1} \gtrsim 400$ GeV, a degenerate stop mass spectrum can also be accommodated.

4.2 Production Cross Sections and Decay Branching Fractions of the SM-like H_1

In Fig. 6, we show the cross section ratios of NMSSM model to the Standard Model ($\sigma \times \text{Br}/\text{SM}$) for $gg \rightarrow H_1 \rightarrow \gamma\gamma$ in panel (a) and $gg \rightarrow H_1 \rightarrow WW/ZZ$ in panel (b) as a function of m_{H_1} . The current 95% C.L. experimental exclusion limits for the SM Higgs searches in the $\gamma\gamma$, WW and ZZ channels are also imposed. While the $\gamma\gamma$ limit imposes strong constraints in the low m_{H_1} region, for m_{H_1} in the mass window of 124 – 128 GeV, the WW and ZZ cross section bounds are more important and rule out points with large $\sigma \times \text{Br}$. For the $\gamma\gamma$ channel, $\sigma \times \text{Br}/\text{SM}$ mainly varies in the range of 0.8 – 1.75, where the lower limit comes from our requirement of the signal region, as indicated by the current Higgs signal at both the ATLAS and CMS experiments [4, 5, 51]. Notice that for a few points, $\sigma \times \text{Br}/\text{SM}$ as large as 2 can be reached. For the WW/ZZ channel, $\sigma \times \text{Br}/\text{SM}$ varies mostly between the range of 0.7 – 1.6, with a few points that could reach a value of 0.5 or even smaller.

In the NMSSM, both the production cross section and decay branching fractions could deviate from their SM values. In the mass window of 124 – 128 GeV, $\sigma(gg \rightarrow H_1)/\sigma_{\text{SM}}$ typically varies between 0.6 – 1.4, although a suppression as small as 0.2 or an enhancement as large as 1.7 are also possible. For the decay branching fraction, $H_1 \rightarrow WW/ZZ$ ($\gamma\gamma$) is typically approximately 0.6–1.5 (0.6–2) of the SM value. There are a few points with very large enhancement factors, approximately 3–4 (5–6) for WW/ZZ ($\gamma\gamma$), which are needed to compensate the associated suppression from the gluon fusion production.

$H_1 \rightarrow \gamma\gamma$ and $H_1 \rightarrow WW/ZZ$ are highly correlated, as in the case of the MSSM scenario. This is because the loop generated $H_1\gamma\gamma$ coupling receives its dominant contribution

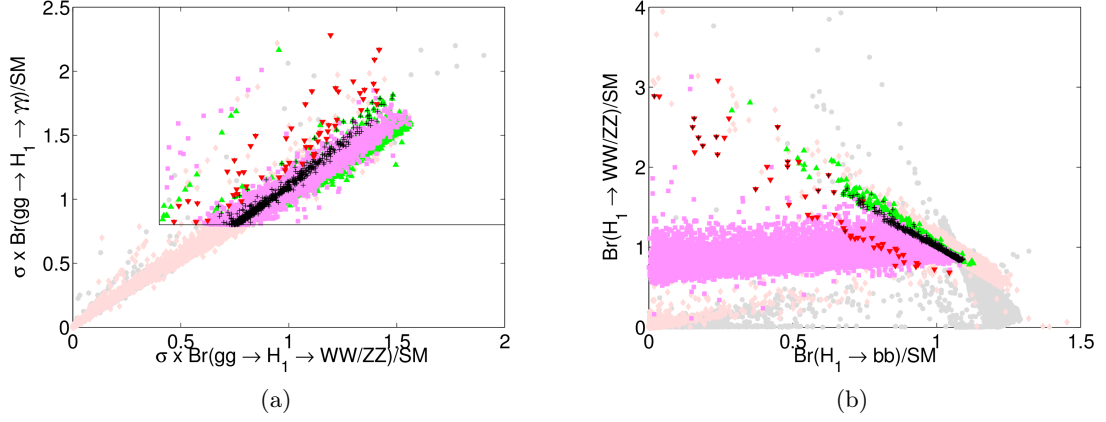


Figure 7. The normalized $\sigma \times \text{Br}/\text{SM}$ for (a) $\gamma\gamma$ versus WW/ZZ channel and (b) the normalized $\text{Br}/\text{Br}_{\text{SM}}$ for WW/ZZ versus bb in the H_1 -126 case. Color coding is the same as for Fig. 5.

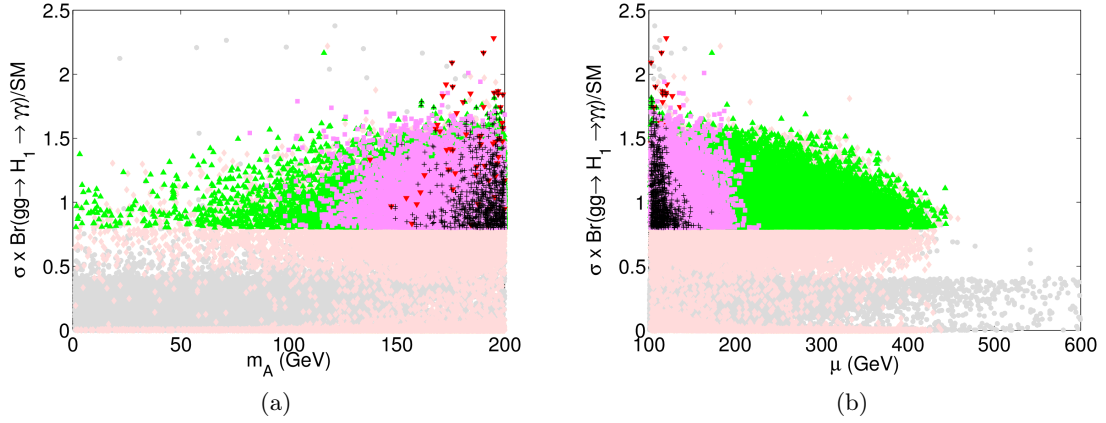


Figure 8. The normalized $\sigma \times \text{Br}/\text{SM}$ for $gg \rightarrow H_1 \rightarrow \gamma\gamma$ with (a) m_A dependence and (b) μ dependence in the H_1 -126 case. Color coding is the same as for Fig. 5.

from the W -loop and is therefore controlled by the same $H_1 WW$ coupling. Such correlation is shown in Fig. 7, panel (a) for $\gamma\gamma$ versus VV . In the H_1 -126 case, most of the points fall into the region of

$$\frac{\sigma \times \text{Br}(gg \rightarrow H_1 \rightarrow \gamma\gamma)/(\sigma \times \text{Br})_{\text{SM}}}{\sigma \times \text{Br}(gg \rightarrow H_1 \rightarrow VV)/(\sigma \times \text{Br})_{\text{SM}}} = \frac{\text{Br}(H_1 \rightarrow \gamma\gamma)/\text{Br}_{\text{SM}}}{\text{Br}(H_1 \rightarrow VV)/\text{Br}_{\text{SM}}} \approx 1.1 \quad . \quad (4.1)$$

However, there are a few scattered points with larger $\gamma\gamma : VV$ ratios. These points have an enhanced $H_1 \rightarrow \gamma\gamma$ partial width due to light stop contributions.

Unlike the correlation shown in the $\gamma\gamma$ versus VV channel, the correlation between the bb and VV channels exhibit interesting feature, as shown in Fig. 7, panel (b), for $\frac{\text{Br}}{\text{Br}_{\text{SM}}}(H_1 \rightarrow bb)$ versus $\frac{\text{Br}}{\text{Br}_{\text{SM}}}(H_1 \rightarrow VV)$. For H_1 Region I, bb and WW are anti-correlated so that the VV channel is enhanced compared to the SM value only when the bb channel gets relatively suppressed. This is as expected since bb and VV are the two dominant H_1 decay channels for $m_{H_1} > 2m_{A_1}$.

For H_1 Region II with low m_{A_1} , however, no such correlation is observed. While $H_1 \rightarrow bb$ could be much suppressed compared to its SM value, $\text{Br}(H_1 \rightarrow VV)/\text{Br}_{\text{SM}}$ varies in the range of 0.5 – 1.5, almost independently of $\text{Br}(H_1 \rightarrow bb)/\text{Br}_{\text{SM}}$. The opening of the $H_1 \rightarrow A_1 A_1$ channel in this mass window replaces $H_1 \rightarrow bb$ to keep $H_1 \rightarrow VV$ in the desired range to satisfy the cross section requirement.

The $\tau\tau$ and bb channels have also been searched for at the LHC, which indicate a weak SM Higgs signal of approximately $1 - 2\sigma$ [49, 50, 53, 54]. For the $\tau\tau$ channel, while the dominant contribution comes from the vector boson fusion (VBF) production, $gg \rightarrow H \rightarrow \tau\tau$ could be separated with a dedicated search [49, 53]. $H \rightarrow bb$ has been studied for both VH and ttH production, with better limits coming from VH associated production [50, 54]. In the NMSSM, since it is the same down-type Higgs H_d that couples to both the bottom quark and the tauon, $H_1 bb$ and $H_1 \tau\tau$ receive the same corrections (up to small difference in the radiative corrections that are non-universal for bottom and tau). Therefore, the bb and $\tau\tau$ channels are highly correlated: $\text{Br}(H_1 \rightarrow bb)/\text{Br}_{\text{SM}} \approx \text{Br}(H_1 \rightarrow \tau\tau)/\text{Br}_{\text{SM}}$. For VBF/VH $\rightarrow H_1 \rightarrow \tau\tau/bb$, $\sigma \times \text{Br}/\text{SM}$ is $\lesssim 1.1$. While for $gg \rightarrow H_1 \rightarrow \tau^+\tau^-$, an enhancement as large as 1.5 of the SM value is possible, which is again from stop loop corrections to $gg \rightarrow H_1$. ttH_1 with $H_1 \rightarrow bb$ receives little enhancement, $\sigma \times \text{Br}/\text{SM} \lesssim 1.05$.

Fig. 8 shows the parameter dependence of $\sigma \times \text{Br}/\text{SM}$ for $gg \rightarrow H_1 \rightarrow \gamma\gamma$ for m_A [panel (a)] and μ [panel (b)]. Larger values for $\sigma \times \text{Br}/\text{SM}$ is achieved for larger values of m_A and smaller values of μ . If a significant enhancement of $gg \rightarrow H_1 \rightarrow \gamma\gamma$ is observed in future experiments, m_A and μ (as well as A_λ) would be restricted to a narrower region.

4.3 Wave Function Overlap

The deviation of the production and decay of H_1 can be traced back to the h_v , H_v and S fractions in H_1 , which is given by the wave function overlap $|\xi_{H_1}^{h_v}|^2$, $|\xi_{H_1}^{H_v}|^2$ and $|\xi_{H_1}^S|^2$, as defined in Eq. (2.13). Fig. 9 shows $|\xi_{H_i}^S|^2$ versus $|\xi_{H_i}^{h_v}|^2$ for H_1 [panel (a)], H_2 [panel (b)] and H_3 [panel (c)]. Since $|\xi_{H_i}^{h_v}|^2 + |\xi_{H_i}^{H_v}|^2 + |\xi_{H_i}^S|^2 = 1$, the distance between the cross diagonal line and the points indicates the value of $|\xi_{H_i}^{H_v}|^2$. For the generic H_1 Region IA (green points), $|\xi_{H_1}^{h_v}|^2 + |\xi_{H_1}^S|^2 \sim 1$; the H_v -fraction in H_1 is almost 0. Typically, about 70% or more of H_1 is h_v , which couples exactly like the SM Higgs, while the singlet component varies between 0 to approximately 30%. For H_2 , it could be either H_v -dominant for those points with $|\xi_{H_2}^S|^2 \sim 0$, or a mixture of H_v and S for points with larger $|\xi_{H_2}^S|^2$. H_3 is mostly singlet-dominant, or with a small mixture of h_v for points close to the cross-diagonal line. It could also have a significant $H_v - S$ mixture for points with smaller $|\xi_{H_3}^S|^2$.

For the H_1 Region IB (red points), $|\xi_{H_1}^{h_v}|^2 < 0.7$, H_1 typically has a sizable fraction of H_v and S . H_2 is also a mixture of h_v , H_v and S , with H_3 being mostly a H_v - S mixture.

For H_1 in the low m_{A_1} region (magenta points of H_1 Region II), H_1 and H_2 are mostly a $h_v - H_v$ mixture, with H_1 being more h_v -like, and H_2 being more H_v -like. This region and Region IB share the property that they typically depend on a suppressed $H_1 b\bar{b}$ coupling proportional to $\xi_{H_i}^{h_v} - \xi_{H_i}^{H_v} \tan\beta$. The S fractions of Region II vary between 0 to 25% for both H_1 and H_2 , while it is the dominant component of H_3 .

Fig. 10 shows the fraction of MSSM CP-odd Higgs A_v in the light CP-odd Higgs A_1 : $|\xi_{A_1}^{A_v}|^2$ as a function of A_κ [panel (a)] and μ [panel (b)]. The more negative A_κ becomes,

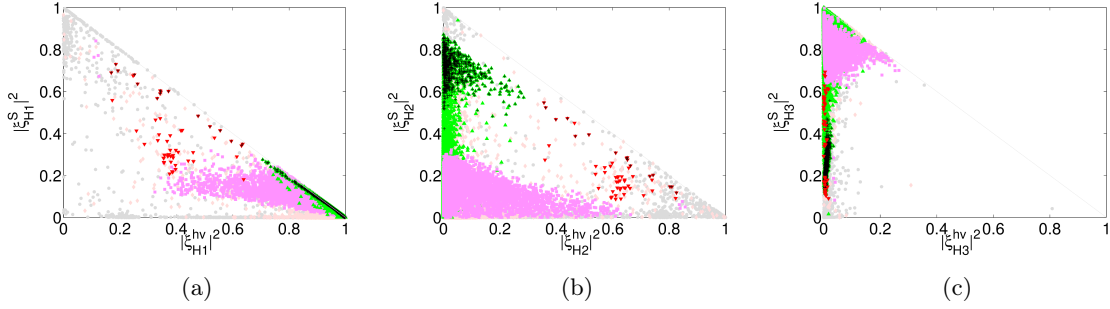


Figure 9. $|\xi_{H_i}^S|^2$ versus $|\xi_{H_i}^{hv}|^2$ for H_1 (a), H_2 (b) and H_3 (c) in the H_1 -126 case. Color coding is the same as for Fig. 5.

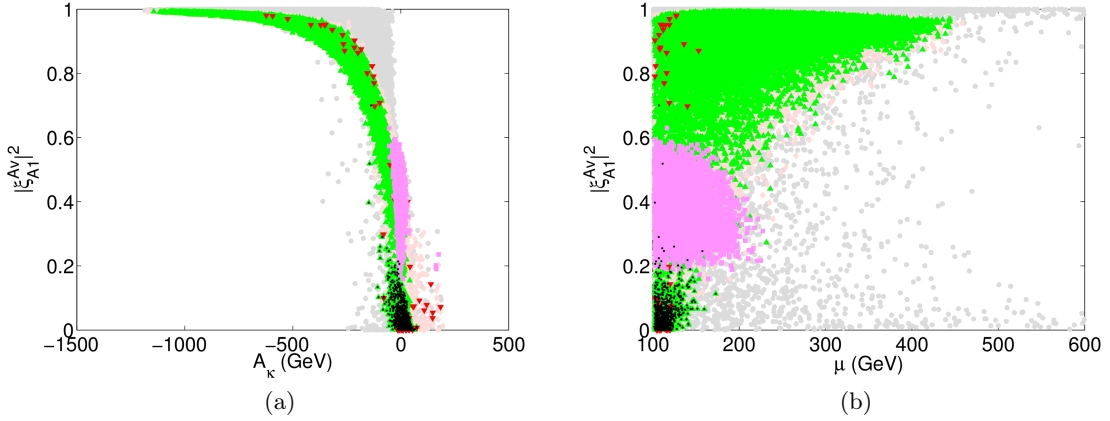


Figure 10. A_v -fraction in the light CP-odd Higgs A_1 : $|\xi_{A_1}^{Av}|^2 = 1 - |\xi_{A_2}^{Av}|^2 = 1 - |\xi_{A_1}^{As}|^2$ in the H_1 -126 case. Color coding is the same as for Fig. 5.

the larger the diagonal mass term $m_{A_s}^2$ for the singlet A_s becomes, which results in A_1 becoming more and more A_v -like. The μ dependence also shows a trend of large μ leading to A_1 being more A_v -like, mainly due to the $-3\kappa/\lambda \mu A_\kappa$ contribution to the $m_{A_s}^2$ mass term. The A_s -fraction in A_1 , as well as the A_v -fraction in A_2 , is simply $1 - |\xi_{A_1}^{As}|^2$. For the points that satisfy the perturbativity requirement (black points), A_1 is mostly singlet like. For regions with small $m_{A_1} < m_{H_1}/2$ (magenta points), a significant fraction of A_1 , 40% to 80%, is singlet. While for generic H_1 Region I, A_1 could be either A_v -like (small m_A , large negative A_κ and A_λ , large μ , large κ) or A_s -like, depending on the NMSSM parameters. Note that while we are focusing on the low m_A region, which controls the mass scale for the MSSM-type CP-odd Higgs, the mass parameter for the CP-odd singlet Higgs could vary in a large range given the scanning parameter region. As a result, m_{A_1} is below 300 GeV, while the mass for the heavy CP-odd Higgs, m_{A_2} , could be as large as 1 TeV or higher.

	$\tan\beta$	m_A (GeV)	μ (GeV)	λ	κ	A_λ (GeV)	A_κ (GeV)
$m_{H_2} \sim 126$	$\gtrsim 1$	0~200	100~300	0~0.75	0~1	-600~300	-1200~50
H_2 -126	1~3.25	100~200	100~200	0.4~0.75	$\gtrsim 0.05$	-300~300	-1200~50
perturb.	1.5~2.5	170~200	100~130	0.5~0.7	0.05~0.6	0~300	-300~50
$m_{H_1} < \frac{m_{H_2}}{2}$	1.25~2.5	125~200	100~150	0.5~0.75	$\gtrsim 0.3$	0~200	-500~-250

Table 3. NMSSM Parameter region for the H_2 -126 case.

5 H_2 as the SM-like Higgs Boson

5.1 Parameter Regions

In the limit where the mixings between h_v , H_v and S are small, there are two cases that give rise to H_2 being SM-like: H_1 being singlet like and H_3 being mostly H_v ; or H_1 being mostly H_v -like and H_3 being mostly singlet. Including the loop corrections as well as mixture between h_v , H_v and S , the separation between these two cases becomes less distinct. The former case is similar to H_1 -126, except that the singlet is now the lightest state. The latter case is similar to the MSSM non-decoupling region, which requires a high level of fine-tuning to satisfy the experimental constraints, as well as mass and cross section requirements. As a result, in the NMSSM, while there are points with a relatively large H_v -fraction in H_1 , there is always a sizable S -fraction in H_1 as well.

Unlike the H_1 -126 case, where imposing the mass window on m_{H_1} already greatly narrows down the parameter regions while the cross section requirement usually does not provide further restriction, imposing the mass window in the H_2 -126 case ($124 \text{ GeV} < m_{H_2} < 128 \text{ GeV}$) does not greatly reduce the parameter space beyond the already restricted space from satisfying the experimental constraints. Requiring H_2 to have a SM-like $gg \rightarrow \gamma\gamma$, WW/ZZ rate, however, does further reduce the parameter space to be in the small $\tan\beta$, small μ , medium to large λ , and small $|A_\lambda|$ region, as summarized in Table 3. Note that compared to the H_1 -126 case, where m_A could be very small, in the H_2 -126 case, m_A is typically larger than about 100 GeV. We note, however, that $m_{A_{loop}}$ in both cases is greater than approximately 150 GeV. In the H_1 -126 case, the SM-like Higgs is pushed down and requires a larger stop-loop correction while in the present H_2 -126 case, the SM-like Higgs is pushed up and, as a result, requires less of a contribution from the stop sector. The stop mass parameters M_{3SQ} , M_{3SU} and A_t are therefore less restricted in the H_2 -126 case.

Also shown in Table 3 is the region where λ and κ remain perturbative until the GUT scale. Unlike the H_1 -126 case in which $|A_t|$ is restricted to be $\gtrsim 1200 \text{ GeV}$, for the H_2 -126 case, $|A_t|$ is typically unrestricted.

While the light CP-odd Higgs A_1 is almost always heavier than $m_{H_2}/2$, the lightest CP-even Higgs H_1 could be lighter than $m_{H_2}/2$ such that the $H_2 \rightarrow H_1 H_1$ decay opens up. Although H_2 is typically h_v -like, it could obtain a relatively large S -fraction to suppress the otherwise dominant decay mode $H_2 \rightarrow bb$. Therefore, we separate the H_2 -126 case into three regions:

- H_2 Region IA: $m_{H_1} > m_{H_2}/2$ and $|\xi_{H_2}^{h_v}|^2 > 0.5$: green points in Figs. 11-14.

- H_2 Region IB: $m_{H_1} > m_{H_2}/2$ and $|\xi_{H_2}^{h_v}|^2 < 0.5$: red points in Figs. 11-14.
- H_2 Region II: $m_{H_1} < m_{H_2}/2$: magenta points in Figs. 11-14.

In Fig. 11, we show the viable regions in various combinations of the NMSSM parameters. The first two panels show the (a) λ versus m_A , and (b) κ versus m_A regions. Small $m_A \lesssim 100$ GeV is not favored since the cross sections for $gg \rightarrow H_2 \rightarrow \gamma\gamma, WW/ZZ$ are suppressed. λ is typically in the range of 0.4 – 0.75. Smaller λ is not allowed due to the suppressed cross sections, while larger values of λ are not allowed due to charged Higgs mass bounds. κ varies over the whole range of 0 – 1, with larger values of m_A preferred for smaller κ .

Panel (c) of Fig. 11 shows the viable region in the λ - κ plane. Regions with small λ satisfy the mass window but fail the cross section requirement. Also, shown in black, are those points that remain perturbative until the Planck scale, which spans a range of λ between 0.5 to 0.7 and κ between 0.1 and 0.5. Panel (d) of Fig. 11 shows the viable region in the $\tan\beta$ - $m_{A_{loop}}$ plane. $\tan\beta$ falls into a range of 1.5 – 3.25, while $m_{A_{loop}}$ varies between 160 – 240 GeV (m_A varies between 100 – 200 GeV).

Panel (e) of Fig. 11 shows a weak correlation between A_λ and μ . Regions of $A_\lambda \lesssim -300$ GeV fail the cross section requirement. There is also a correlation between A_κ and μ , as shown in panel (f) of Fig. 11. This is because in the H_2 -126 case, most H_1 are singlet-like. The CP-even singlet mass needs to be smaller than m_{h_v} and is typically controlled by the cancellation between a positive μ parameter and a negative A_κ term, as shown in Eq. (2.11). This correlation can be seen more clearly in H_2 Region II (magenta points) where finer cancellation is enforced.

The magenta points in Fig. 11 are for H_2 Region II: $m_{H_1} < m_{H_2}/2$. They span the region of small $|A_\kappa|, |A_\lambda|$ and μ , intermediate $\kappa, m_A \sim 200$ GeV, and $1.5 \lesssim \tan\beta \lesssim 2$, as summarized in Table 3.

5.2 Production Cross Sections and Decay Branching Fractions for the SM-like H_2

The ranges of $\sigma \times \text{Br}/\text{SM}$ for $gg \rightarrow H_2 \rightarrow \gamma\gamma$, shown in Fig. 12, is slightly large than that of the H_1 -126 case. An enhancement as large as a factor of 2 can be achieved in the present case. For $gg \rightarrow H_2 \rightarrow WW/ZZ$, the $\sigma \times \text{Br}/\text{SM}$ is typically in the range of 0.4 – 1.6, and bounded above by the current experimental searches in the WW/ZZ channels. Note that a relatively strong suppression of about 0.4 could be accommodated more easily than in the H_1 -126 case.

$H_2 \rightarrow \gamma\gamma$ and $H_2 \rightarrow WW/ZZ$ are also highly correlated, as shown in Fig. 13, panel (a) for $\gamma\gamma$ versus WW/ZZ . There are several branches, corresponding to H_2 Region IA and IB as categorized in Sec. 5.1. For Region IA (green points) with H_2 being mostly h_v -dominant, $\frac{\text{Br}(H_1 \rightarrow \gamma\gamma)/(\text{Br})_{\text{SM}}}{\text{Br}(H_1 \rightarrow WW)/(\text{Br})_{\text{SM}}} \approx 1.1$ for the lower branch of green points. However, there is another branch with a higher value of $\frac{\text{Br}(H_1 \rightarrow \gamma\gamma)/(\text{Br})_{\text{SM}}}{\text{Br}(H_1 \rightarrow WW)/(\text{Br})_{\text{SM}}} \approx 2$. Those points typically have an enhanced $H_2 \rightarrow \gamma\gamma$ compared to the SM value due to the light stop contributions. For Region IB (red points) with H_2 being a mixture of h_v, H_v and S , $\frac{\text{Br}(H_1 \rightarrow \gamma\gamma)/(\text{Br})_{\text{SM}}}{\text{Br}(H_1 \rightarrow WW)/(\text{Br})_{\text{SM}}} \approx 1.4$.

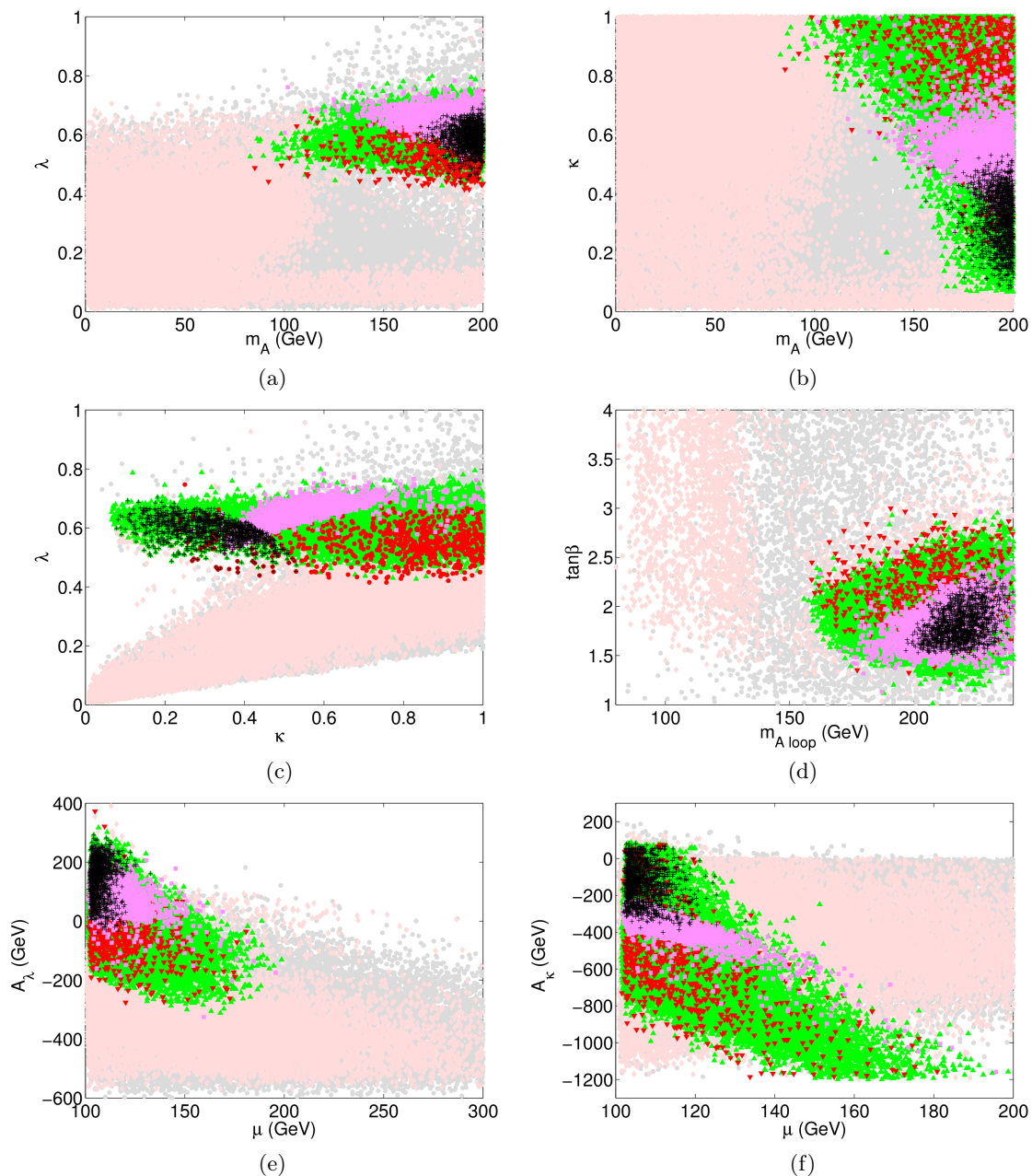


Figure 11. Viable NMSSM parameter regions in the H_2 -126 case: (a) λ versus m_A , (b) κ versus m_A , (c) λ versus κ , (d) $\tan\beta$ versus $m_{A_{loop}}$, (e) A_λ versus μ , and (f) A_κ versus μ . Grey points are those that pass the experimental constraints, pale-pink points are those with H_2 in the mass window $124 \text{ GeV} < m_{H_2} < 128 \text{ GeV}$. Green points are for H_2 Region IA: $m_{H_1} > m_{H_2}/2$ with $|\xi_{H_2}^{h_\nu}|^2 > 0.5$. Red points are for H_2 Region IB: $m_{H_1} > m_{H_2}/2$ with $|\xi_{H_2}^{h_\nu}|^2 < 0.5$. Magenta points are for H_2 Region II: $m_{H_1} < m_{H_2}/2$. The black points are those where λ and κ remain perturbative up to the GUT scale.

In Fig. 13, panel (b), we show the correlation between the bb and VV channel: $\text{Br}(H_2 \rightarrow bb)/\text{Br}_{\text{SM}}$ versus $\text{Br}(H_2 \rightarrow VV)/\text{Br}_{\text{SM}}$. While most regions exhibit an anti-correlation as

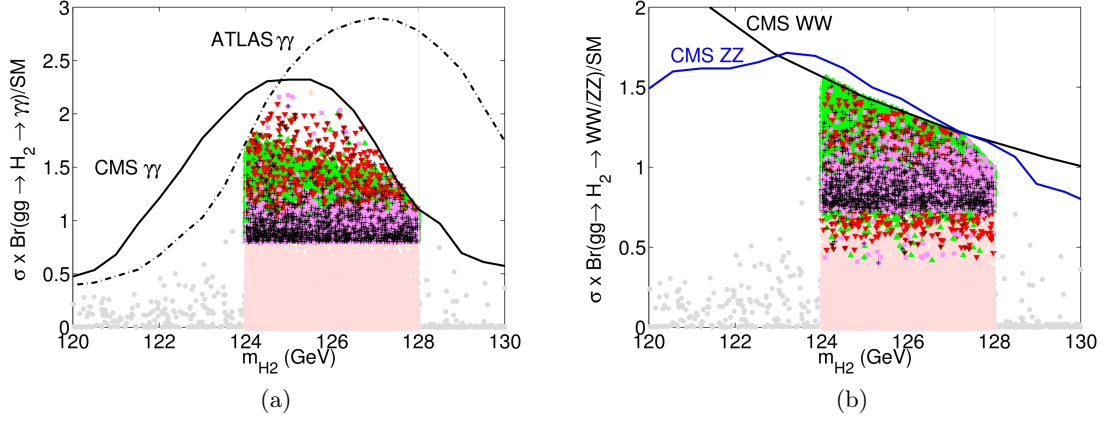


Figure 12. The normalized $\sigma \times \text{Br}/\text{SM}$ for (a) $gg \rightarrow H_2 \rightarrow \gamma\gamma$ and (b) $gg \rightarrow H_2 \rightarrow WW/ZZ$ as a function of m_{H_2} in the H_2 -126 case. The current experimental constraints from the SM Higgs searches of the $\gamma\gamma$, WW and ZZ channels are also imposed. Color coding is the same as for Fig. 11.

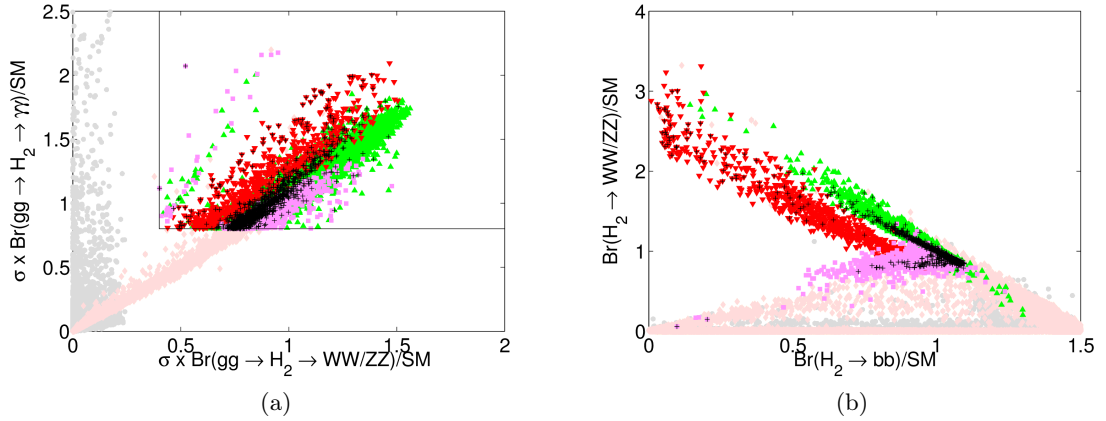


Figure 13. The normalized $\sigma \times \text{Br}/\text{SM}$ for (a) $\gamma\gamma$ versus WW/ZZ channel, and the normalized $\text{Br}/\text{Br}_{\text{SM}}$ for (b) WW/ZZ versus bb in the H_2 -126 case. Color coding is the same as for Fig. 11.

expected, in H_2 Region II (magenta points) with $m_{H_1} < m_{H_2}/2$, the branching fraction for the VV channel is almost independent of the bb channel. This is, similar to the magenta region in the H_1 -126 case, due to an opening up of the decay channel $H_2 \rightarrow H_1 H_1$, which compensates for the suppression of the bb channel while keeping the total decay width of H_2 close to the SM value.

The bb and $\tau\tau$ channels also exhibit a similar correlation behavior as in the H_1 -126 case: $\text{Br}(H_2 \rightarrow bb)/\text{Br}_{\text{SM}} \approx \text{Br}(H_2 \rightarrow \tau\tau)/\text{Br}_{\text{SM}}$. For VBF and VH with $H_2 \rightarrow \tau\tau, bb$, $\sigma \times \text{Br}/\text{SM}$ is in the range of 0.4 – 1.1 for H_2 Region IA and is much suppressed in Region IB and is $\lesssim 0.4$. For $gg \rightarrow H_2 \rightarrow \tau^+\tau^-$, most of the H_2 Region IA falls into the range of 0.4 – 1.4, although an enhancement as large as 2 is possible. For Region IB, this channel is almost always suppressed with $\sigma \times \text{Br} \lesssim 0.8(\sigma \times \text{Br})_{\text{SM}}$. The process ttH_2 with $H_2 \rightarrow bb$ receives little enhancement, with $\sigma \times \text{Br}/\text{SM} \lesssim 1.06$ for Region IA and $\sigma \times \text{Br}/\text{SM} \lesssim 0.7$

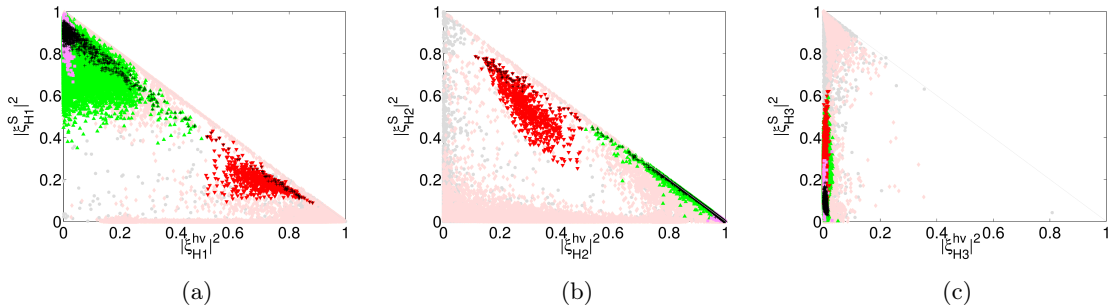


Figure 14. $|\xi_{H_i}^S|^2$ versus $|\xi_{H_i}^{h_v}|^2$ for H_1 (a), H_2 (b) and H_3 (c) in the H_2 -126 case. Color coding is the same as for Fig. 11.

for Region IB.

5.3 Wave Function Overlap

Fig. 14 shows $|\xi_{H_i}^S|^2$ versus $|\xi_{H_i}^{h_v}|^2$ for (a) H_1 , (b) H_2 and (c) H_3 . For H_2 Region II (magenta points), H_1 is mostly singlet, H_2 is mostly h_v and H_3 is mostly H_v .

For H_2 region IA (green points) with $|\xi_{H_2}^{h_v}|^2 > 0.5$, while H_2 is mostly h_v -like by definition, its H_v -fraction is almost always small. In contrast, while H_1 is dominated by S , it could have a relatively large H_v -fraction. H_3 is typically a mixture of S and H_v , with the H_v -fraction always being sizable: $|\xi_{H_3}^{H_v}|^2 \gtrsim 0.4$. The h_v -fraction in H_3 is almost negligible.

For H_2 region IB (red points) with $|\xi_{H_2}^{h_v}|^2 < 0.5$, the singlet fraction in H_2 could be significant, sometime even as large as 0.8. While the h_v -fraction in H_2 decreases, it increases accordingly in H_1 : $|\xi_{H_1}^{h_v}|^2 > 0.5$. This opens up the possibility of H_1 with sizable $H_1 WW/H_1 ZZ$ couplings that we will discuss in the next section. Both H_1 and H_2 could have a fraction of H_v as large as 0.3–0.4. H_3 , on the other hand, is mostly a mixture of H_v and S , with the h_v -fraction being negligible.

The compositions of A_1 and A_2 are similar to that of the H_1 -126 case. Larger negative values of A_κ lead to a large fraction of A_1 being A_v . However, for $A_\kappa \sim 0$, A_1 could be mostly A_s .

6 LHC Phenomenology for the Non-SM-like Higgs Bosons

In the previous sections, we have presented two very interesting scenarios in the low- m_A region. The SM-like Higgs boson could be the lightest scalar particle (H_1 -126) while the next lightest one is an admixture of its MSSM partner and the singlet state. The alternative is that the SM-like Higgs boson is the second lightest (H_2 -126) while the lightest scalar is a H_v - S - h_v mixture. While the collider phenomenology of the SM-like Higgs boson has been shown earlier, it would be interesting to identify the signal features of the other low-mass Higgs bosons.

6.1 H_1 as the SM-like Higgs Boson

In Fig. 15(a), we show the dominant production cross sections of gg fusion and VBF for H_1 (red and pink points), H_2 (green and light green points) and H_3 (blue and light blue

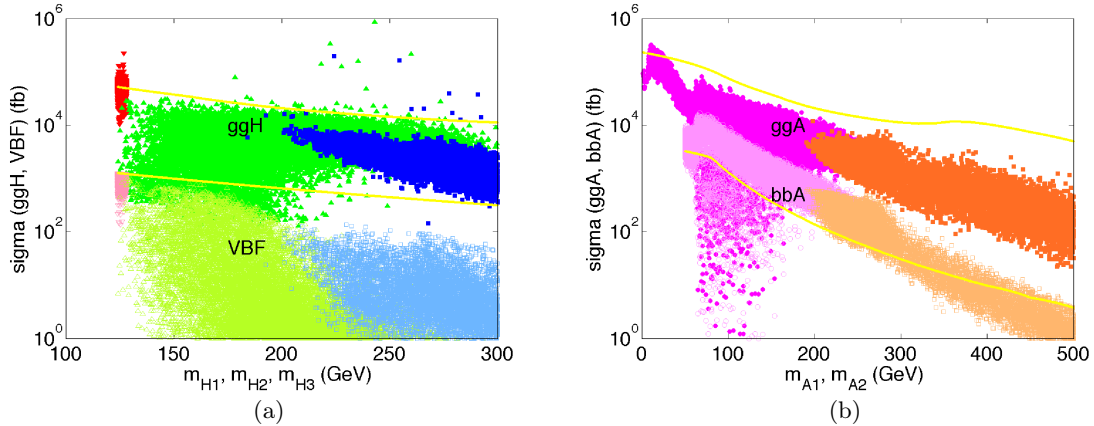


Figure 15. Cross sections at the 14 TeV LHC in the H_1 -126 case for (a) $H_{1,2,3}$ production via gg fusion (VBF) denoted by red (pink), green (light green), blue (light blue) points, respectively, and for (b) $A_{1,2}$ production via gg fusion ($b\bar{b}$ fusion) denoted by purple (light purple), brown (light brown) points, respectively. The yellow lines indicate the cross sections with SM couplings.

points), respectively, satisfying all the constraints for the H_1 -126 case at the 14 TeV LHC. The yellow lines indicate the corresponding cross sections with SM couplings. When the h_v -fraction is sizable, the production cross sections for H_2 could be similar to the SM-like rate. The cross sections could also be suppressed by two orders of magnitudes if the S -fraction is large, as for the H_3 case. The VBF process can be more significantly suppressed than that of gg fusion. The production cross section for the CP-odd states $A_{1,2}$ from gg fusion via triangle loop diagrams is shown in Fig. 15(b). The rate can be similar to that of the SM-like Higgs boson and the spread of the cross section over the parameter scan is roughly about an order of magnitude, less pronounced than those for the CP-even cases. Although about an order magnitude lower, the production cross section from $b\bar{b}$ annihilation can be significantly larger than that of the SM value, due to the $\tan\beta$ enhancement.

In Fig. 16, we further show the relevant branching fractions for $H_{1,2,3}$, $A_{1,2}$ and H^\pm to the SM particles (and $H_{2,3} \rightarrow \tilde{t}_1\tilde{t}_1$) for the case of H_1 -126. The yellow lines indicate the corresponding branching fraction values with SM couplings. The non SM-like Higgs bosons typically have suppressed decay branching fractions to the regular SM channels, in particular for H_3 , due to the opening up of new decay channels to lighter Higgs bosons pairs. The experimental searches for those new Higgs bosons at the LHC will continue to cover a broad parameter region. A_1 decays dominantly to $b\bar{b}$, with about 10% to $\tau^+\tau^-$, as shown in Fig. 16(e). The phenomenological consequences of this decay have been studied in the literature [32, 56–58], emphasizing the $h \rightarrow A_1A_1 \rightarrow 4\tau, 4b, 2\tau 2b$ modes and we will not discuss them further here. One of the most striking results for the CP-odd Higgs decay, perhaps, is the potentially very large enhancement for the branching fraction $A_1 \rightarrow \gamma\gamma$, as seen in Fig. 16(e). This is partly because of the reduced Γ_{tot} caused by the suppression of the $A_1b\bar{b}$ coupling, and partly because of the enhanced $\Gamma(A_1 \rightarrow \gamma\gamma)$ due to the loop contributions from the light charginos and charged Higgs bosons, and from the top and stop. In the pure singlet limit, the dominant viable decay channel is $A_1 \rightarrow \gamma\gamma$ induced

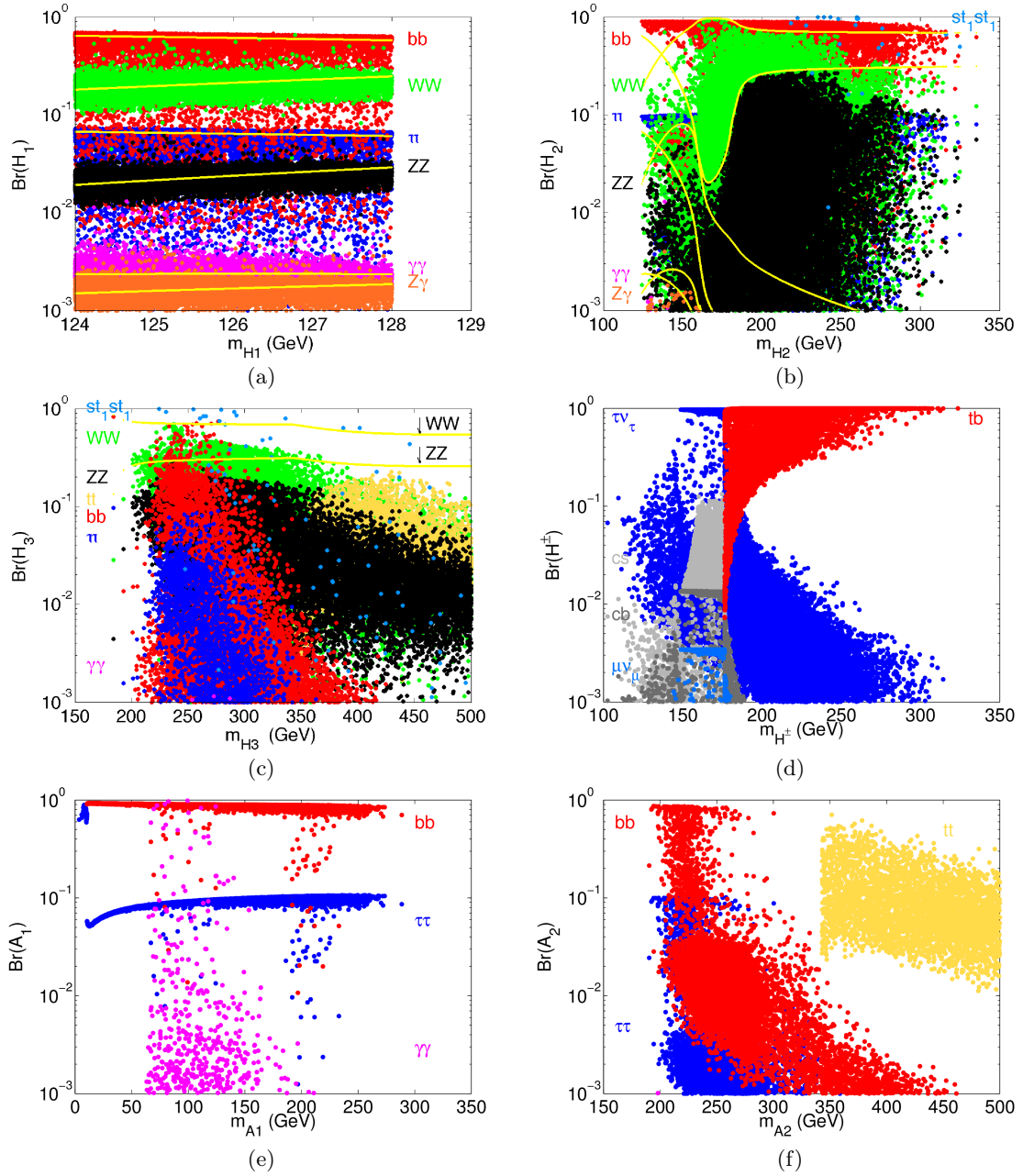


Figure 16. Decay branching fractions for $H_{1,2,3}$, $A_{1,2}$ and H^\pm to the SM particles (and $H_{2,3} \rightarrow \tilde{t}_1 \tilde{t}_1$) in the case of H_1 -126. The yellow lines indicate the corresponding values with the SM couplings.

by the chargino loop and charged Higgs loop from their non-suppressed couplings with the singlet. However, the chargino in our case is always much lighter than the charged Higgs, granting non-zero $A_1 \gamma \gamma$ coupling. The total width could be as low as around 10^{-6} GeV. This may lead to interesting scenarios with a proper LSP that produces a greatly suppressed low-end $\gamma \gamma$ continuum for an indirect dark matter search [59] such as Fermi-LAT.

Another interesting feature is that the CP-even heavy Higgs bosons could decay to a

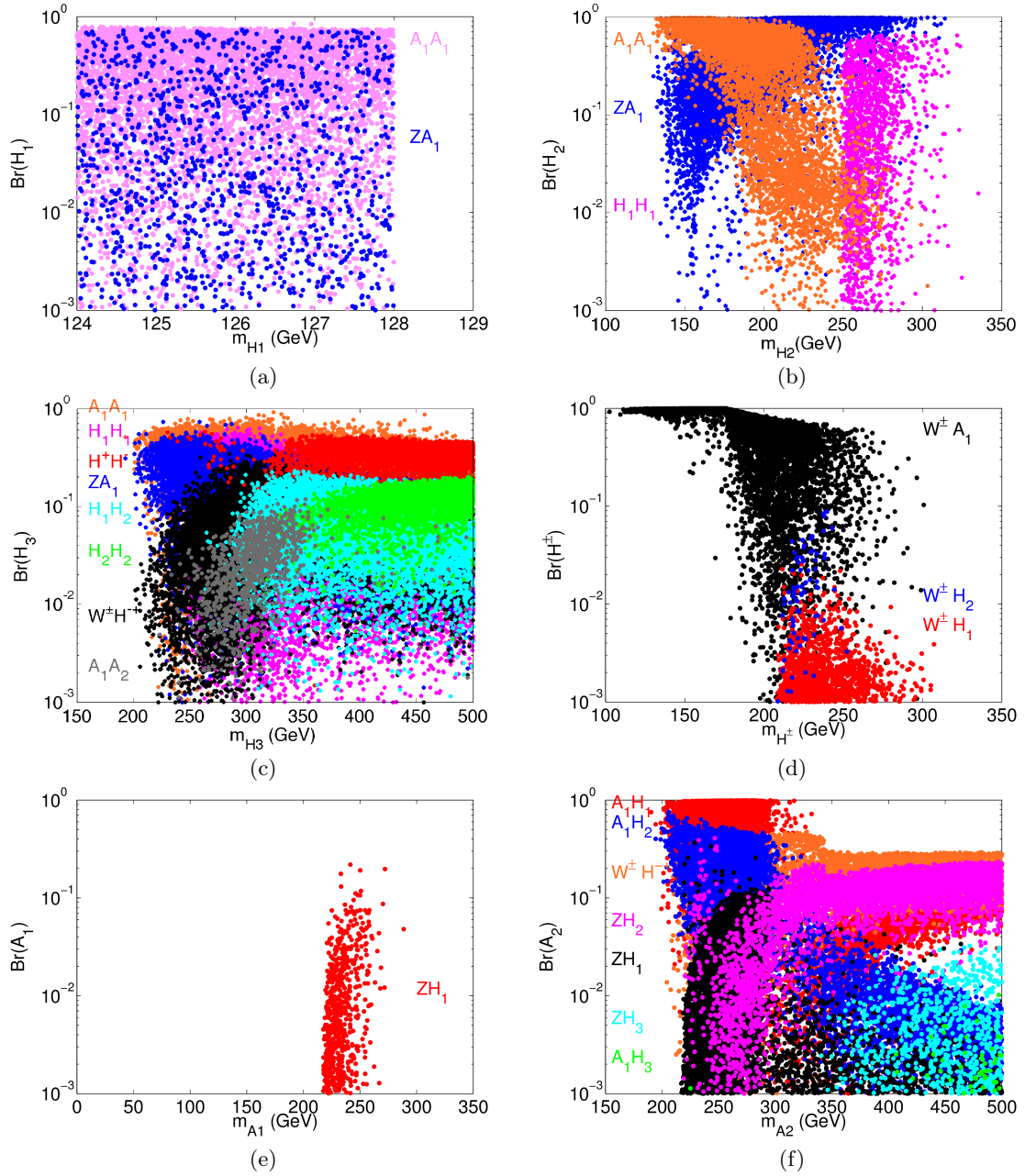


Figure 17. Decay branching fractions for $H_{1,2,3}$, $A_{1,2}$ and H^\pm to Higgs bosons in the case of H_1 -126.

pair of stops when kinematically accessible. It is important to note that a heavier Higgs boson could decay to a pair of lighter Higgs bosons at a substantial rate and sometimes dominantly, as long as kinematically accessible. As shown in Fig. 17 for the case of H_1 -126,

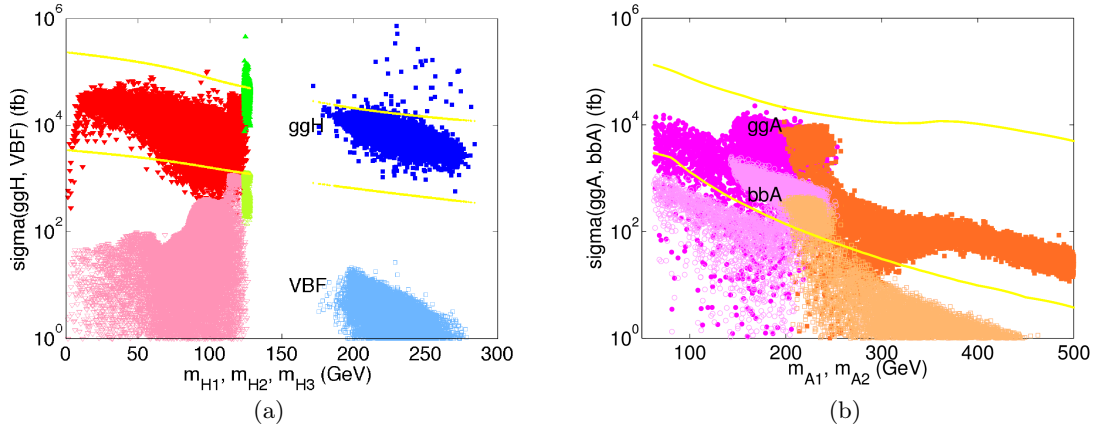


Figure 18. Cross sections at the 14 TeV LHC in the H_2 -126 case. The color codes and the legends are the same as in Fig. 15.

we see that

$$H_1 \rightarrow A_1 A_1, \quad Z A_1, \quad (6.1)$$

$$H_2 \rightarrow A_1 A_1, \quad Z A_1, \quad H_1 H_1, \quad (6.2)$$

$$H_3 \rightarrow A_1 A_1, \quad H_1 H_1, \quad Z A_1, \quad W^\pm H^\mp, \quad A_1 A_2, \quad H_1 H_2, \quad H_2 H_2, \quad H^+ H^-, \quad (6.3)$$

$$H^\pm \rightarrow W^\pm A_1, \quad W^\pm H_2, \quad W^\pm H_1, \quad (6.4)$$

$$A_1 \rightarrow Z H_1, \quad (6.5)$$

$$A_2 \rightarrow A_1 H_1, \quad A_1 H_2, \quad W^\pm H^\mp, \quad Z H_1, \quad Z H_2, \quad Z H_3, \quad A_1 H_3, \quad (6.6)$$

roughly according to the sizes of the branching fractions at the low values of the mass. The relative branching fractions depend on phase space factors and the couplings dictated by the MSSM and singlet components. Consequently, the striking signals will be multiple heavy quarks, such as $4b$, $4t$ and $2b2t$, and will likely include $\tau^+\tau^-$ as well. While the final state with a W or Z may be a good channel from the event identification view point, the final states with multiple heavy quarks may be rather challenging to separate out from the large SM backgrounds.

6.2 H_2 as the SM-like Higgs Boson

Similar results for the Higgs production and decay channels are shown in Figs. 18–20, respectively, at the 14 TeV LHC for the H_2 -126 case. It is interesting to note that H_1 is non-SM-like, and lighter than H_2 , yet it could have as large a production cross section as H_2 . Although the branching fractions to WW , ZZ , and $\gamma\gamma$ are somewhat smaller than those for the SM, these clean signals can be searched for in the near future. For example, the H_1 could have a sufficient coupling with vector boson pairs to be responsible for the approximately 98 GeV excess at LEP [28, 60, 61].

Again, we find it very interesting that a heavier Higgs state could dominantly decay to a pair of lighter Higgs bosons. Note that H_1 is non-SM-like and light, so that there are no

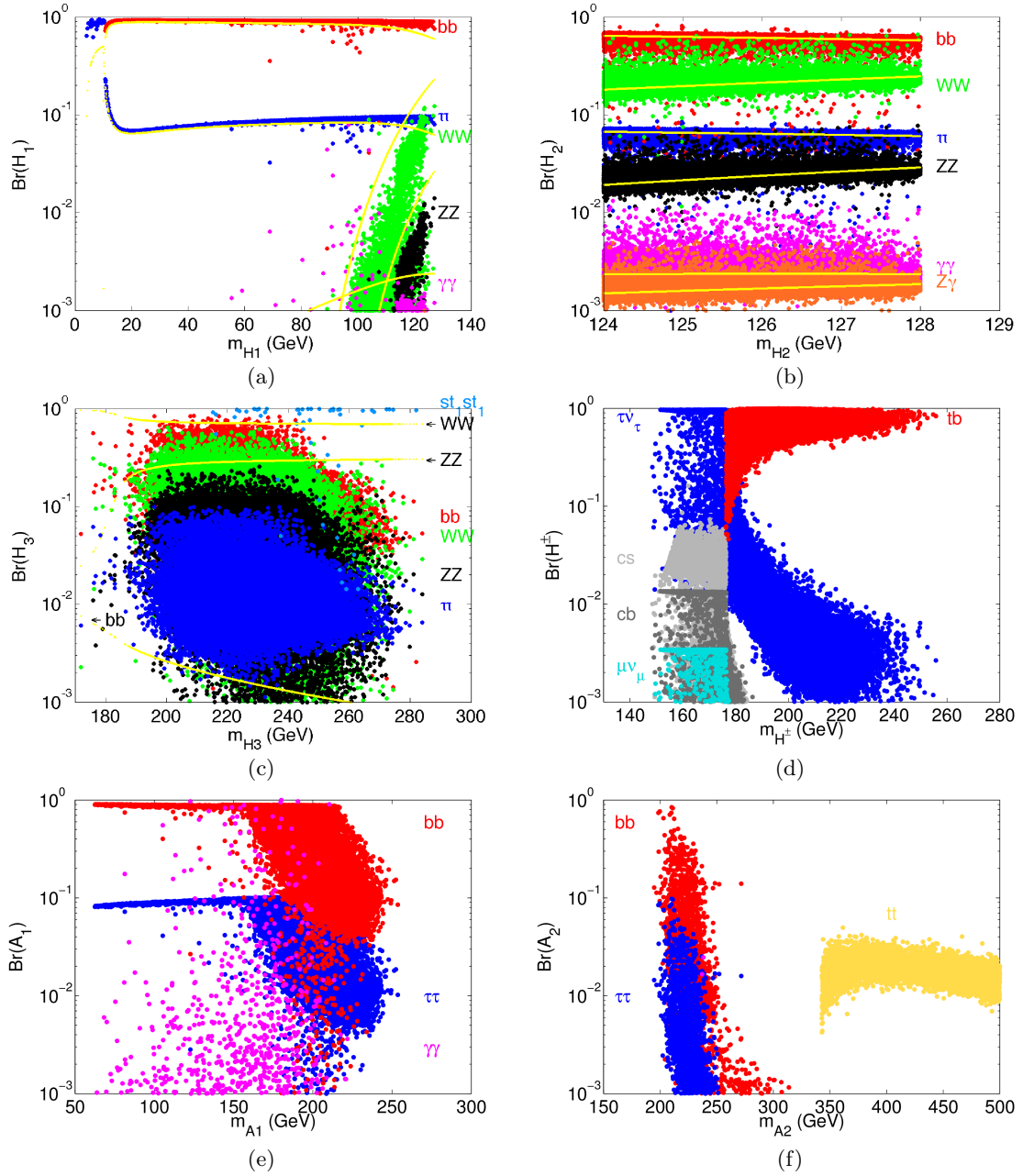


Figure 19. Decay branching fractions for $H_{1,2,3}$, $A_{1,2}$ and H^\pm to the SM particles (and $H_3 \rightarrow \tilde{t}_1 \tilde{t}_1$) in the case of H_2 -126. The yellow lines indicate the corresponding values with the SM couplings.

Higgs pair channels for it to decay to. We see, from Fig. 20,

$$H_2 \rightarrow H_1 H_1, \quad (6.7)$$

$$H_3 \rightarrow H_1 H_1, \quad H_1 H_2, \quad Z A_1, \quad A_1 A_1, \quad H_2 H_2, \quad (6.8)$$

$$H^\pm \rightarrow W^\pm H_1, \quad W^\pm A_1, \quad W^\pm H_2, \quad (6.9)$$

$$A_1 \rightarrow Z H_1, \quad Z H_2, \quad (6.10)$$

$$A_2 \rightarrow Z H_1, \quad A_1 H_1, \quad A_1 H_2, \quad Z H_2, \quad W^\pm H^\mp, \quad Z H_3, \quad A_1 H_3, \quad (6.11)$$

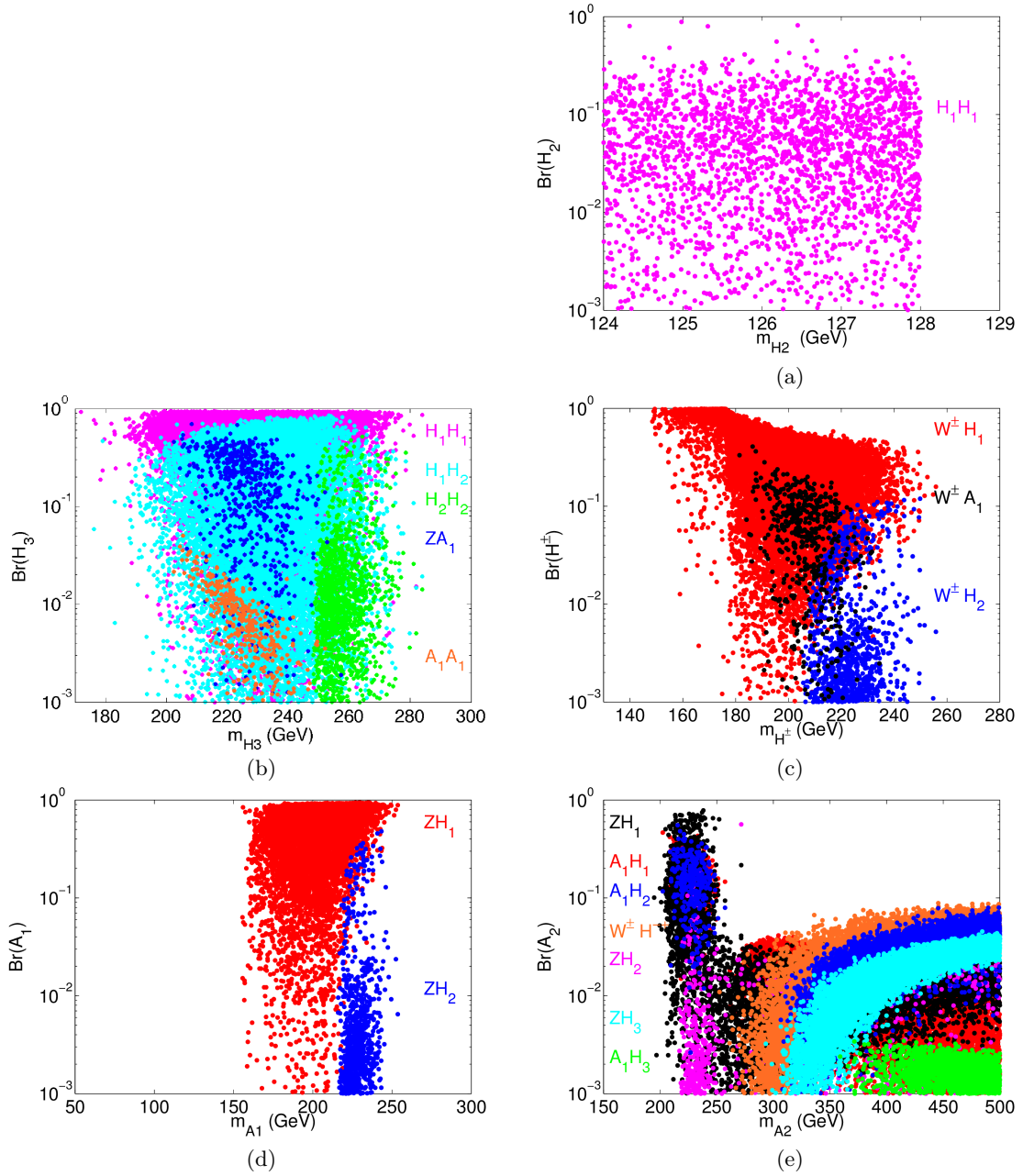


Figure 20. Decay branching fractions for $H_{1,2,3}$, $A_{1,2}$ and H^\pm to Higgs bosons in the case of H_2 -126.

again roughly according to the sizes of the branching fractions at the low values of the mass. The collider signatures would be multiple heavy quarks, τ 's, and multiple gauge bosons as commented in the last section. The Higgs pair final states from the decay may serve as an important window for a new discovery.

It was previously noted [16, 62] that in the low- m_A region, the direct production of the Higgs boson pairs may be quite accessible at the LHC due to the model-independent

gauge couplings for $H^+H^-\gamma$ and $H^\pm AW^\mp$. Additional studies include processes such as $H_3 \rightarrow H_2H_1$ [63], low mass H^\pm with light A_1 [64], two low mass Higgs scenarios [65] and Higgs boson pair productions [66].

7 Summary and Conclusions

In the framework of the Next to Minimal Supersymmetric Standard Model, we study the Higgs sector in light of the discovery of the SM-like Higgs boson at the LHC. We pay particular attention to the light Higgs states in the case when the parameter $m_A \lesssim 2m_Z$. Our results, coming from a broad parameter scan after implementing the current collider constraints from Higgs physics, lead to the following findings:

- The Higgs bosons in the NMSSM, namely three CP-even states, two CP-odd states, and two charged Higgs states, could all be rather light, near or below the electroweak scale (v), although the singlet-like state can be heavier. The SM-like Higgs boson could be either the lightest CP-even scalar as in Fig. 3(a), or the second lightest CP-even scalar as in Fig. 3(c), but is unlikely to be the heaviest scalar as in Fig. 3(e).
- If we relax the perturbativity requirement by allowing the NMSSM parameters λ and κ to be larger (see Tables 2 and 3), the allowed region for the mass parameters would be enlarged significantly (e.g., black versus green, red and magenta points in Fig. 4, Fig. 5 and Fig. 11, etc.).
- The SM-like Higgs signal at the LHC may be appreciably modified, as seen in Figs. 15(a) and 18(a) for production, and Figs. 16(a) and 19(b) for decay.
- Consequently, the $\gamma\gamma$ rate can be enhanced (Figs. 6, 8 and 12). The naive correlations of $\gamma\gamma/VV$ and $VV/b\bar{b}$ ratios can be violated (Figs. 7 and 13). Furthermore, if the SM-like Higgs can decay to a pair of lighter Higgs bosons, the anti-correlation in the $VV/b\bar{b}$ ratio can be further broken (magenta regions of Figs. 7(b) and 13(b)).
- New Higgs bosons beyond the SM may be readily produced at the LHC. The production cross sections via gg fusion and VBF could be of the same orders of magnitude as those of the SM productions (Figs. 15 and 18). Their decay branching fractions to the SM particles could be even larger than those of the SM (Figs. 16 and 19), depending on $\tan\beta$ and the size of their SM-like Higgs fractions (Figs. 9 and 14).
- The unique channels for the heavy Higgs signal are the decays to a pair of light Higgs bosons (Figs. 17 and 20). The striking signals will be multiple heavy quarks (t , b) and tau-leptons in the final states.

In conclusion, the Higgs sector in the NMSSM provides a well motivated theoretical framework consistent with the Higgs boson discovery and the searches at the LHC. The low- m_A parameter region yields multiple light Higgs bosons that lead to rich phenomenology at colliders. Although strongly constrained by the current searches, it is also highly predictive. Dedicated studies for this very interesting sector, in particular for a multiple Higgs boson

final state at the LHC, will allow a search for this scenario to be completed in the near future.

Acknowledgments

The work of N.C., T.H. and Z.L. was supported in part by the U.S. Department of Energy under grant No. DE-FG02-95ER40896, in part by PITT PACC, and in part by the LHC-TI under U.S. National Science Foundation, grant NSF-PHY-0705682. The work of S.S. was supported by the Department of Energy under Grant DE-FG02-04ER-41298. T.H. and S.S. would also like to thank the Aspen Center for Physics for the hospitality during which part of this work was carried out. ACP is supported by NSF under grant 1066293.

References

- [1] J. R. Ellis, J. Gunion, H. E. Haber, L. Roszkowski, and F. Zwirner, *Higgs Bosons in a Nonminimal Supersymmetric Model*, *Phys.Rev.* **D39** (1989) 844.
- [2] M. Drees, *Supersymmetric Models with Extended Higgs Sector*, *Int.J.Mod.Phys.* **A4** (1989) 3635.
- [3] H. P. Nilles, M. Srednicki and D. Wyler, *Weak Interaction Breakdown Induced by Supergravity*, *Phys. Lett. B* **120**, 346 (1983); J. E. Kim and H. P. Nilles, *The mu Problem and the Strong CP Problem*, *Phys. Lett. B* **138**, 150 (1984); J. M. Frere, D. R. T. Jones and S. Raby, *Fermion Masses and Induction of the Weak Scale by Supergravity*, *Nucl. Phys. B* **222**, 11 (1983); G. F. Giudice and A. Masiero, *A Natural Solution to the mu Problem in Supergravity Theories*, *Phys. Lett. B* **206**, 480 (1988).
- [4] **ATLAS** Collaboration, G. Aad et al., *Observation of a new particle in the search for the Standard Model Higgs boson with the ATLAS detector at the LHC*, *Phys.Lett.* **B716** (2012) 1–29, [[arXiv:1207.7214](#)].
- [5] **CMS** Collaboration, S. Chatrchyan et al., *Observation of a new boson at a mass of 125 GeV with the CMS experiment at the LHC*, *Phys.Lett.* **B716** (2012) 30–61, [[arXiv:1207.7235](#)].
- [6] L. J. Hall, D. Pinner, and J. T. Ruderman, *A Natural SUSY Higgs Near 126 GeV*, *JHEP* **1204** (2012) 131, [[arXiv:1112.2703](#)].
- [7] M. Carena, S. Gori, N. R. Shah, and C. E. Wagner, *A 125 GeV SM-like Higgs in the MSSM and the $\gamma\gamma$ rate*, *JHEP* **1203** (2012) 014, [[arXiv:1112.3336](#)].
- [8] H. Baer, V. Barger, P. Huang, and X. Tata, *Natural Supersymmetry: LHC, Dark Matter and ILC Searches*, *JHEP* **1205** (2012) 109, [[arXiv:1203.5539](#)].
- [9] M. W. Cahill-Rowley, J. L. Hewett, A. Ismail, and T. G. Rizzo, *The Higgs Sector and Fine-Tuning in the pMSSM*, *Phys.Rev.* **D86** (2012) 075015, [[arXiv:1206.5800](#)].
- [10] S. F. King, M. Muhlleitner, R. Nevzorov, and K. Walz, *Natural NMSSM Higgs Bosons*, *Nucl.Phys.* **B870** (2013) 323–352, [[arXiv:1211.5074](#)].
- [11] K. Agashe, Y. Cui, and R. Franceschini, *Natural Islands for a 125 GeV Higgs in the Scale-Invariant NMSSM*, *JHEP* **1302** (2013) 031, [[arXiv:1209.2115](#)].
- [12] H. E. Haber, *Nonminimal Higgs Sectors: The Decoupling Limit and Its Phenomenological Implications*, [hep-ph/9501320](#).

- [13] **ATLAS** Collaboration, G. Aad et al., *Search for neutral MSSM Higgs bosons decaying to $\tau^+\tau^-$ pairs in proton-proton collisions at $\sqrt{s} = 7$ TeV with the ATLAS detector*, *Phys.Lett.* **B705** (2011) 174–192, [[arXiv:1107.5003](#)].
- [14] **ATLAS** Collaboration, G. Aad et al., *Search for Neutral MSSM Higgs bosons in $\sqrt{s}=7$ TeV pp collisions at ATLAS*, Tech. Rep. ATLAS-CONF-2012-094, CERN, Geneva, Jul, 2012.
- [15] **CMS** Collaboration, S. Chatrchyan et al., *Search for a Higgs Boson Decaying into a b-quark Pair and Produced in Association with b Quarks in Proton-Proton Collisions at 7 TeV*, [arXiv:1302.2892](#).
- [16] N. D. Christensen, T. Han, and S. Su, *MSSM Higgs Bosons at The LHC*, *Phys.Rev.* **D85** (2012) 115018, [[arXiv:1203.3207](#)].
- [17] U. Ellwanger, *A Higgs Boson near 125 GeV with Enhanced Di-photon Signal in the NMSSM*, *JHEP* **1203** (2012) 044, [[arXiv:1112.3548](#)].
- [18] S. King, M. Muhlleitner, and R. Nevzorov, *NMSSM Higgs Benchmarks Near 125 GeV*, *Nucl.Phys.* **B860** (2012) 207–244, [[arXiv:1201.2671](#)].
- [19] J.-J. Cao, Z.-X. Heng, J. M. Yang, Y.-M. Zhang, and J.-Y. Zhu, *A SM-like Higgs near 125 GeV in Low Energy SUSY: a Comparative Study for MSSM and NMSSM*, *JHEP* **1203** (2012) 086, [[arXiv:1202.5821](#)].
- [20] J. F. Gunion, Y. Jiang, and S. Kraml, *The Constrained NMSSM and Higgs near 125 GeV*, *Phys.Lett.* **B710** (2012) 454–459, [[arXiv:1201.0982](#)].
- [21] U. Ellwanger and C. Hugonie, *Higgs Bosons near 125 GeV in the NMSSM with Constraints at the GUT scale*, *Adv.High Energy Phys.* **2012** (2012) 625389, [[arXiv:1203.5048](#)].
- [22] K. Choi, S. H. Im, K. S. Jeong, and M. Yamaguchi, *Higgs Mixing and Diphoton Rate Enhancement in NMSSM Models*, [arXiv:1211.0875](#).
- [23] K. S. Jeong, Y. Shoji, and M. Yamaguchi, *Singlet-Doublet Higgs Mixing and Its Implications on the Higgs Mass in the PQ-NMSSM*, *JHEP* **1209** (2012) 007, [[arXiv:1205.2486](#)].
- [24] T. Graf, R. Grober, M. Muhlleitner, H. Rzehak, and K. Walz, *Higgs Boson Masses in the Complex NMSSM at One-Loop Level*, *JHEP* **1210** (2012) 122, [[arXiv:1206.6806](#)].
- [25] K. Kowalska, S. Munir, L. Roszkowski, E. M. Sessolo, S. Trojanowski, et al., *The Constrained NMSSM with a 125 GeV Higgs Boson – A Global Analysis*, [arXiv:1211.1693](#).
- [26] D. A. Vasquez, G. Belanger, C. Boehm, J. Da Silva, P. Richardson, et al., *The 125 GeV Higgs in the NMSSM in Light of LHC Results and Astrophysics Constraints*, *Phys.Rev.* **D86** (2012) 035023, [[arXiv:1203.3446](#)].
- [27] D. E. Lopez-Fogliani, *Light Higgs and Neutralino Dark Matter in the NMSSM*, *J.Phys.Conf.Ser.* **384** (2012) 012014.
- [28] G. Belanger, U. Ellwanger, J. F. Gunion, Y. Jiang, S. Kraml, et al., *Higgs Bosons at 98 and 125 GeV at LEP and the LHC*, *JHEP* **1301** (2013) 069, [[arXiv:1210.1976](#)].
- [29] G. Belanger, U. Ellwanger, J. Gunion, Y. Jiang, and S. Kraml, *Two Higgs Bosons at the Tevatron and the LHC?*, [arXiv:1208.4952](#).
- [30] J. F. Gunion, Y. Jiang, and S. Kraml, *Could two NMSSM Higgs Bosons be Present near 125 GeV?*, *Phys.Rev.* **D86** (2012) 071702, [[arXiv:1207.1545](#)].
- [31] D. Miller, R. Nevzorov, and P. Zerwas, *The Higgs Sector of the Next-to-Minimal Supersymmetric Standard Model*, *Nucl.Phys.* **B681** (2004) 3–30, [[hep-ph/0304049](#)].

- [32] V. Barger, P. Langacker, H. -S. Lee and G. Shaughnessy, *Higgs Sector in Extensions of the MSSM*, *Phys. Rev.* **D73**, 115010 (2006) [[hep-ph/0603247](#)].
- [33] **LEP Higgs Working Group** for Higgs boson searches, **ALEPH** Collaboration, **DELPHI** Collaboration, **L3** Collaboration, **OPAL** Collaboration, *Search for charged Higgs bosons: Preliminary combined results using LEP data collected at energies up to 209-GeV*, [hep-ex/0107031](#).
- [34] **ALEPH** Collaboration, A. Heister et al., *Search for charged Higgs bosons in e^+e^- collisions at energies up to $\sqrt{s} = 209\text{-GeV}$* , *Phys.Lett.* **B543** (2002) 1–13, [[hep-ex/0207054](#)].
- [35] S. Heinemeyer, O. Stal, and G. Weiglein, *Interpreting the LHC Higgs Search Results in the MSSM*, *Phys.Lett.* **B710** (2012) 201–206, [[arXiv:1112.3026](#)].
- [36] A. Arbey, M. Battaglia, A. Djouadi, and F. Mahmoudi, *The Higgs sector of the Phenomenological MSSM in the Light of the Higgs boson Discovery*, *JHEP* **1209** (2012) 107, [[arXiv:1207.1348](#)].
- [37] R. Benbrik, M. Gomez Bock, S. Heinemeyer, O. Stal, G. Weiglein, et al., *Confronting the MSSM and the NMSSM with the Discovery of a Signal in the Two Photon Channel at the LHC*, *Eur.Phys.J.* **C72** (2012) 2171, [[arXiv:1207.1096](#)].
- [38] K. Hagiwara, J. S. Lee, and J. Nakamura, *Properties of 125 GeV Higgs Boson in Non-decoupling MSSM Scenarios*, *JHEP* **1210** (2012) 002, [[arXiv:1207.0802](#)].
- [39] J. Ke, H. Luo, M.-x. Luo, K. Wang, L. Wang, et al., *Revisit to Non-decoupling MSSM*, [arXiv:1211.2427](#).
- [40] M. Drees, *A Supersymmetric Explanation of the Excess of Higgs-Like Events at the LHC and at LEP*, *Phys.Rev.* **D86** (2012) 115018, [[arXiv:1210.6507](#)].
- [41] **CMS** Collaboration, S. Chatrchyan et al., *Search for a light charged Higgs boson in top quark decays in pp collisions at $\sqrt{s} = 7\text{ TeV}$* , *JHEP* **1207** (2012) 143, [[arXiv:1205.5736](#)].
- [42] **ATLAS** Collaboration, G. Aad et al., *Search for charged Higgs bosons decaying via $H^+ \rightarrow \tau\nu$ in top quark pair events using pp collision data at $\sqrt{s} = 7\text{ TeV}$ with the ATLAS detector*, *JHEP* **1206** (2012) 039, [[arXiv:1204.2760](#)].
- [43] **ATLAS** Collaboration, G. Aad et al., *Search for a light charged Higgs boson in the decay channel $H^+ \rightarrow c\bar{s}$ in $t\bar{t}$ events using pp collisions at $\sqrt{s} = 7\text{ TeV}$ with the ATLAS detector*, [arXiv:1302.3694](#).
- [44] M. Carena, S. Gori, N. R. Shah, C. E. Wagner, and L.-T. Wang, *Light Stau Phenomenology and the Higgs gamma gamma Rate*, *JHEP* **1207** (2012) 175, [[arXiv:1205.5842](#)].
- [45] U. Ellwanger, J. F. Gunion, and C. Hugonie, *NMHDECAY: A Fortran Code for the Higgs Masses, Couplings and Decay Widths in the NMSSM*, *JHEP* **0502** (2005) 066, [[hep-ph/0406215](#)].
- [46] U. Ellwanger and C. Hugonie, *NMHDECAY 2.0: An Updated Program for Sparticle Masses, Higgs Masses, Couplings and Decay Widths in the NMSSM*, *Comput.Phys.Commun.* **175** (2006) 290–303, [[hep-ph/0508022](#)].
- [47] G. Belanger, F. Boudjema, C. Hugonie, A. Pukhov, and A. Semenov, *Relic Density of Dark Matter in the NMSSM*, *JCAP* **0509** (2005) 001, [[hep-ph/0505142](#)].
- [48] **ATLAS** Collaboration, G. Aad et al., *Search for the Standard Model Higgs boson produced in association with top quarks in proton-proton collisions at $\sqrt{s} = 7\text{TeV}$ using the ATLAS*

detector, Tech. Rep. ATLAS-CONF-2012-135, CERN, Geneva, Sep, 2012; *Update of the $H \rightarrow WW^{(*)} \rightarrow e \nu \mu \nu$ analysis with 13.0 fb⁻¹ of $\sqrt{s} = 8$ TeV data collected with the ATLAS detector*, Tech. Rep. ATLAS-CONF-2012-158, CERN, Geneva, Nov, 2012; *Updated ATLAS results on the signal strength of the Higgs-like boson for decays into WW and heavy fermion final states*, Tech. Rep. ATLAS-CONF-2012-162, CERN, Geneva, Nov, 2012; *Study of the channel $H \rightarrow Z^* Z \rightarrow \ell^+ \ell^- q \bar{q}$ in the mass range 120–180 GeV with the ATLAS Detector at $\sqrt{s} = 7$ TeV*, Tech. Rep. ATLAS-CONF-2012-163, CERN, Geneva, Nov, 2012; *Updated results and measurements of properties of the new Higgs-like particle in the four lepton decay channel with the ATLAS detector*, Tech. Rep. ATLAS-CONF-2012-169, CERN, Geneva, Dec, 2012; *An update of combined measurements of the new Higgs-like boson with high mass resolution channels*, Tech. Rep. ATLAS-CONF-2012-170, CERN, Geneva, Dec, 2012.

- [49] **ATLAS** Collaboration, G. Aad et al., *Search for the Standard Model Higgs boson in $H \rightarrow \tau^+ \tau^-$ decays in proton-proton collisions with the ATLAS detector*, Tech. Rep. ATLAS-CONF-2012-160, CERN, Geneva, Nov, 2012.
- [50] **ATLAS** Collaboration, G. Aad et al., *Search for the Standard Model Higgs boson produced in association with a vector boson and decaying to bottom quarks with the ATLAS detector*, Tech. Rep. ATLAS-CONF-2012-161, CERN, Geneva, Nov, 2012.
- [51] **ATLAS** Collaboration, G. Aad et al., *Observation and study of the Higgs boson candidate in the two photon decay channel with the ATLAS detector at the LHC*, Tech. Rep. ATLAS-CONF-2012-168, CERN, Geneva, Dec, 2012.
- [52] **CMS** Collaboration, S. Chatrchyan et al., *Search for Higgs boson production in association with top quark pairs in pp collisions*, Tech. Rep. CMS-PAS-HIG-12-025, CERN, Geneva, 2012; *Updated results on the new boson discovered in the search for the standard model Higgs boson in the ZZ to 4 leptons channel in pp collisions at $\sqrt{s} = 7$ and 8 TeV*, Tech. Rep. CMS-PAS-HIG-12-041, CERN, Geneva, 2012; *Evidence for a particle decaying to $W^+ W^-$ in the fully leptonic final state in a standard model Higgs boson search in pp collisions at the LHC*, Tech. Rep. CMS-PAS-HIG-12-042, CERN, Geneva, 2012; *Combination of standard model Higgs boson searches and measurements of the properties of the new boson with a mass near 125 GeV*, Tech. Rep. CMS-PAS-HIG-12-045, CERN, Geneva, 2012.
- [53] **CMS** Collaboration, S. Chatrchyan et al., *Higgs to tau tau (SM) (HCP)*, Tech. Rep. CMS-PAS-HIG-12-043, CERN, Geneva, 2012.
- [54] **CMS** Collaboration, S. Chatrchyan et al., *Search for the standard model Higgs boson produced in association with W or Z bosons, and decaying to bottom quarks for HCP 2012*, Tech. Rep. CMS-PAS-HIG-12-044, CERN, Geneva, 2012.
- [55] **CMS** Collaboration, S. Chatrchyan et al., *Higgs to tau tau (MSSM) (HCP)*, Tech. Rep. CMS-PAS-HIG-12-050, CERN, Geneva, 2012.
- [56] R. Dermisek and J. F. Gunion, *Consistency of LEP event excesses with an $h \rightarrow aa$ decay scenario and low-fine-tuning NMSSM models*, *Phys.Rev.* **D73** (2006) 111701, [[hep-ph/0510322](https://arxiv.org/abs/hep-ph/0510322)].
- [57] R. Dermisek and J. F. Gunion, *The NMSSM Close to the R-symmetry Limit and Naturalness in $h \rightarrow aa$ Decays for $m(a) < 2m(b)$* , *Phys.Rev.* **D75** (2007) 075019, [[hep-ph/0611142](https://arxiv.org/abs/hep-ph/0611142)].
- [58] M. Carena, T. Han, G.-Y. Huang, and C. E. Wagner, *Higgs Signal for $h \rightarrow aa$ at Hadron Colliders*, *JHEP* **0804** (2008) 092, [[arXiv:0712.2466](https://arxiv.org/abs/hep-ph/0712.2466)].

- [59] G. Chalons, M. J. Dolan, and C. McCabe, *Neutralino dark matter and the Fermi gamma-ray lines*, *JCAP* **1302** (2013) 016, [[arXiv:1211.5154](#)].
- [60] **ALEPH** Collaboration, **DELPHI** Collaboration, **L3** Collaboration, **OPAL** Collaboration, **LEP Working Group** for Higgs Boson Searches Collaboration, S. Schael et al., *Search for neutral MSSM Higgs bosons at LEP*, *Eur.Phys.J.* **C47** (2006) 547–587, [[hep-ex/0602042](#)].
- [61] **LEP Working Group** for Higgs boson searches, **ALEPH** Collaboration, **DELPHI** Collaboration, **L3** Collaboration, **OPAL** Collaboration, R. Barate et al., *Search for the standard model Higgs boson at LEP*, *Phys.Lett.* **B565** (2003) 61–75, [[hep-ex/0306033](#)].
- [62] N. D. Christensen, T. Han, and T. Li, *Pair Production of MSSM Higgs Bosons in the Non-decoupling Region at the LHC*, *Phys.Rev.* **D86** (2012) 074003, [[arXiv:1206.5816](#)].
- [63] Z. Kang, J. Li, T. Li, D. Liu, and J. Shu, *Probing the CP-even Higgs Sector via $H_3 \rightarrow H_2 H_1$ in the Natural NMSSM*, [arXiv:1301.0453](#).
- [64] J. Rathsmann and T. Rossler, *Closing the Window on Light Charged Higgs Bosons in the NMSSM*, *Adv.High Energy Phys.* **2012** (2012) 853706, [[arXiv:1206.1470](#)].
- [65] D. G. Cerdeno, P. Ghosh, and C. B. Park, *Probing the two light Higgs scenario in the NMSSM with a low-mass pseudoscalar*, [arXiv:1301.1325](#).
- [66] J. Cao, Z. Heng, L. Shang, P. Wan, and J. M. Yang, *Pair Production of a 125 GeV Higgs Boson in MSSM and NMSSM at the LHC*, [arXiv:1301.6437](#).